AIMS Mathematics

https://www.aimspress.com/journal/Math

AIMS Mathematics, 11(7): 22277–22315.
DOI: 10.3934/math.2026902
Received: 11 May 2026
Revised: 06 July 2026
Accepted: 15 July 2026
Published: 24 July 2026

Research article

Approximation with a hybrid DD Stancu operator: Applications to coronary vessel visualization, image representation, and geometric modeling

Emine Güven[1] and Nazmiye Gönül Bilgin[2,*]

[1] Graduate School of Natural and Applied Sciences, Zonguldak Bülent Ecevit University, Turkey
[2] Department of Mathematics, Faculty of Science, Zonguldak Bülent Ecevit University, Turkey

* **Correspondence:** Email: nazmiyegonul@beun.edu.tr.

Abstract: This study presents a generalization of the DD Stancu operator reported in the literature by combining it with the lambda Bernstein operator. Using the basis functions of the proposed operator, geometric modeling applications related to vascular visualization, botanical form representation, and entomological form modeling are presented; thus, the role of approximation theory in mathematical modeling and the aforementioned fields is emphasized. The biological modeling and botanical illustration generated using the basis functions of the operator demonstrate the effectiveness of the method in representing organic shapes by enabling the λ-parameter to capture with high precision the natural forms of leaves and butterflies, their internal curves, and venation structures. The model, developed to represent structural changes such as narrowing and widening in vascular geometry, was designed solely as a geometric visualization tool rather than as a validated medical simulation or diagnostic method, and is made available for further studies.

Keywords: Bézier-type curve; λ-modification; double summation operator; linear positive operators; approximation theory; geometric modeling
Mathematics Subject Classification: 41A35, 41A36, 65D17, 68U07

1. Introduction

Approximation theory emerged in the late nineteenth century with Weierstrass's theorem, which states that every continuous function on a closed interval can be uniformly approximated as closely as desired as shown in [1]. Bernstein later provided a constructive proof of this theorem by developing a practical method for constructing approximating polynomials using concepts from probability theory [2,3].

In 1959, Paul de Casteljau and, later, in 1962, Pierre Bézier independently studied mathematical representations of automobile bodies [4,5]. These developments led to Bézier curves, which are based on Bernstein polynomials and can be intuitively controlled by designers through control points. The partition of unity property of the Bernstein basis functions ensures that the curve remains within the region defined by the control points, while the variation-diminishing property limits undesired oscillations relative to the control polygon [6]. These curves, now known as Bézier curves, derived from Bernstein polynomials, have become essential tools in diverse fields such as automotive design, typography, computer graphics, animation, and engineering [7].

Subsequently, in line with requirements from mathematics and applied sciences, the field was expanded with different perspectives to improve the speed and quality of convergence. In 1930, Kantorovich produced a modification by taking the integrals of the functions instead of their values [8]. In 1937, Chlodowsky presented a modification applicable to functions defined on an infinite interval [9]. Approximately thirty years later, Durrmeyer developed a modification based on integrals involving both the basis functions and the function being approximated [10]. In 1968, Stancu introduced additional parameters to improve the flexibility of the approximation process, control the rate of convergence, and reduce boundary effects [11].

In 1997, Phillips extended the theory to q-calculus by using q-integers instead of standard integers in the operator he defined [12]. Another important development was the extension of approximation operators to infinite intervals. Szász-Mirakyan and Baskakov examined the operators they defined in this context [13,14]. Phillips and Schurer conducted studies aimed at increasing the rate of convergence by introducing parameters into their operators [15]. In 2010, Gadjiev and Ghorbanalizadeh developed Stancu-type modifications for both univariate and bivariate cases by improving the parametric structure, which allows faster adaptation to the continuity properties of functions and provides better control over the convergence behavior [16]. The combination of existing approximation operators with fuzzy theory has also contributed to the development of various hybrid operator frameworks [17]. Studies based on post-quantum calculus have also introduced important operator classes and provided a basis for further interdisciplinary research [18–20].

To address the requirements of different fields, researchers have developed more flexible operators, particularly by incorporating additional parameters. These developments have contributed to the discipline through Stancu-type operators and their generalizations. In this regard, several important generalizations of the Stancu operator have been introduced [21–24].

Among the significant extensions of the Bernstein operator, the λ-Bernstein operator plays a notable role. In 2010, Ye et al. defined the λ-Bernstein operator using linear combinations of the classical Bernstein basis functions [25]. For the parameter $\lambda \in [-1,1]$, this operator can improve the rate of convergence without changing the control points of the curve or surface and may reduce endpoint errors. The λ-Bernstein operator has recently attracted considerable attention and has inspired the construction of various related operators [26–30].

Recent developments in intelligent systems, image processing, and mathematical modeling have increased the need for flexible approximation tools. In accordance with previous studies, the present paper aims to address a gap in the literature by combining the DD Stancu operator introduced in [22] with the λ-Bernstein modification proposed in [25]. In this context, the main properties and theoretical structure of the proposed operator are examined in detail. Furthermore, selected application-oriented examples involving visual data representation and vascular geometry visualization are presented to illustrate the applicability of the proposed operator from both theoretical and geometric modeling perspectives.

In this study, the application-oriented geometric models are constructed using the basis-function structure associated with the proposed operator, together with selected control points. Since the operator in Definition 3.3 is generated through the product of two basis functions, these basis functions determine the weighting mechanism used in the Bézier-type representation. Thus, the resulting curves and surfaces are not intended as independent standard Bézier drawings but rather as geometric visualizations influenced by the basis structure of the proposed hybrid operator.

Highlights

* This study combines modified DD Stancu and λ-Bernstein operators within an interdisciplinary approximation-theoretic framework.

* The proposed parametric operator satisfies the conditions of Korovkin-type convergence.

* It provides flexible geometric control for representing structural variations in vascular geometry.

* It connects approximation theory with geometric modeling, vascular visualization, botanical form representation, and entomological form modeling.

* The model enables flexible geometric representation of natural leaf structures and butterfly wing forms, including inner curves and vein-like structures.

The study is organized as follows: Section 2 presents the basic definitions and preliminary results required for the study. In Section 3, a new operator is introduced by incorporating the λ-Bernstein modification into the DD Stancu operator introduced in 2022. It is shown that this operator satisfies the required conditions for Korovkin-type convergence, thus guaranteeing its suitability from the perspective of approximation theory. Furthermore, the properties that the basis functions must satisfy in Bézier-type curve constructions are examined in detail, and the results are supported by graphical illustrations. In Section 4, geometric models based on the defined λ-basis functions are presented to illustrate selected vascular geometry variations, such as narrowing and widening, in the context of coronary vessel visualization. The final section is devoted to discussing the research findings and conclusions reached.

2. Background and preliminaries

An important development occurred in 2010, when Gadjiev and Ghorbanalizadeh refined Stancu-type modifications for both univariate and bivariate cases by improving the parametric structure. These modifications offered a more flexible framework for approximation operators, allowing them to capture a wider range of functional behaviors. Since 2015, several variants of these operators have been introduced and extensively studied in the literature. For example, Acar and Aral examined weighted approximation properties based on the modifications of Gadjiev and Ghorbanalizadeh and obtained stronger convergence results by combining them with classical Bernstein-Chlodowsky structures [31]. Mursaleen et al. focused on q-Bernstein-Stancu-type operators, revealing a more symmetric and efficient structure through moment and central moment analyses [32]. Furthermore, Yang et al. investigated multivariate Stancu operators defined on a simplex and established their approximation properties, demonstrating convergence behavior and effectiveness in approximating multivariate functions [33]. Lin et al. studied the modified λ-Bernstein-Stancu operators and established their main approximation and convergence properties [34]. Gupta introduced and studied a Kantorovich variant of Stancu operators and established their approximation properties, including convergence behavior and error estimates within the framework of positive linear operators [35]. In 2022, Guven and Bilgin defined a two-parameter Stancu-Gadjiev operator and examined its important approximation properties. These studies indicate that Stancu-type modifications play an important role in modern approximation theory, from both theoretical and applied perspectives.

The basic definitions and preliminary results relevant to this study are presented first.

The following definition recalls the operator introduced in [22], whose λ-modification is introduced in the next section. Throughout this section, it is assumed that

$$\frac{\alpha_2}{n+\beta_2} \le x \le \frac{n+\alpha_2}{n+\beta_2},\ 0 \le \alpha_2 \le \alpha_1 \le \beta_1 \le \beta_2 \text{ and } n > \alpha\beta.$$

Definition 2.1.

$$P_{\beta,j}(x) = \binom{\beta}{j}\left(x - \frac{\alpha_2}{n+\beta_2}\right)^j \left(\frac{n+\alpha_2}{n+\beta_2} - x\right)^{\beta-j},$$

$$P_{n-\alpha\beta,k}(x) = \binom{n-\alpha\beta}{k}\left(x - \frac{\alpha_2}{n+\beta_2}\right)^k \left(\frac{n+\alpha_2}{n+\beta_2} - x\right)^{n-\alpha\beta-k},$$

the operator $N_{n,\alpha,\beta}\colon C\left[\frac{\alpha_2}{n+\beta_2},\frac{n+\alpha_2}{n+\beta_2}\right] \to C\left[\frac{\alpha_2}{n+\beta_2},\frac{n+\alpha_2}{n+\beta_2}\right]$ is defined as

$$N_{n,\alpha,\beta}(f,x) = \left(\frac{n}{n+\beta_2}\right)^{(\alpha-1)\beta-n} \sum_{k=0}^{n-\alpha\beta} P_{n-\alpha\beta,k}(x) \sum_{j=0}^{\beta} P_{\beta,j}(x) f\left(\frac{k+j\alpha_1}{n+\beta_1}\right). \tag{1}$$

This operator is referred to as the two-parameter Stancu-Gadjiev operator in [22]. The following equalities hold [22].

$$i)\ \sum_{j=0}^{\beta} P_{\beta,j}(x) = \sum_{j=0}^{\beta} \binom{\beta}{j}\left(x - \frac{\alpha_2}{n+\beta_2}\right)^j \left(\frac{n+\alpha_2}{n+\beta_2} - x\right)^{\beta-j} = \left(\frac{n}{n+\beta_2}\right)^{\beta}$$

$$ii)\ \sum_{k=0}^{n-\alpha\beta} P_{n-\alpha\beta,k}(x) = \sum_{k=0}^{n-\alpha\beta} \binom{n-\alpha\beta}{k}\left(x - \frac{\alpha_2}{n+\beta_2}\right)^k \left(\frac{n+\alpha_2}{n+\beta_2} - x\right)^{n-\alpha\beta-k}$$

$$= \left(\frac{n}{n+\beta_2}\right)^{n-\alpha\beta}$$

Some important properties of the basis functions used in the analysis of this operator are presented in the following lemmas.

Definition 2.2. The original Bezier curve with control points P_i is defined by

$$P(t) = \sum_{i=0}^{n} B_{i,n}(t)\, P_i,$$

where

$$B_{i,n}(t) = \binom{n}{i} t^i (1-t)^{n-i} \qquad t \in [0,1]$$

is the Bernstein basis function of degree n.

For $n \geq 2$ and $t \in [0,1]$, the Bézier basis functions with a shape parameter are defined by

$$\tilde{B}_{0,n}(t) = B_{0,n}(t) - \lambda \frac{1}{n+1} B_{1,n+1}(t),$$

$$\tilde{B}_{i,n}(t) = B_{i,n}(t) + \lambda \left(\frac{n-2i+1}{n^2-1} B_{i,n+1}(t) - \frac{n-2i-1}{n^2-1} B_{i+1,n+1}(t)\right),$$

$$\tilde{B}_{n,n}(t) = B_{n,n}(t) - \lambda \frac{1}{n+1} B_{n,n+1}(t),$$

where $\lambda \in [-1,1]$ is the shape parameter [25].

Definition 2.3. A Bézier curve with a shape parameter and control points P_i is defined by

$$\tilde{P}(t) = \sum_{i=0}^{n} P_i \tilde{B}_{i,n}(t), \qquad t \in [0,1],$$

where $\tilde{B}_{i,n}(t)$ denotes the Bézier basis function with the shape parameter λ [25].

Lemma 2.1. For all $j = 0,1,\dots,\beta$,

$$P_{\beta,j}(x) = \left(\frac{n+\beta_2}{n}\right)\left[\frac{\beta+1-j}{\beta+1} P_{\beta+1,j}(x) + \frac{1+j}{\beta+1} P_{\beta+1,j+1}(x)\right].$$

Lemma 2.2. For $n - \alpha\beta \in \mathbb{N}$ and $x \in \left[\frac{\alpha_2}{n+\beta_2}, \frac{n+\alpha_2}{n+\beta_2}\right]$ for every $k \in 0,1,\dots,n-\alpha\beta$

$$P_{n-\alpha\beta,k}(x) = \frac{n+\beta_2}{n}\left[\frac{n-\alpha\beta+1-k}{n-\alpha\beta+1} P_{n-\alpha\beta+1,k}(x) + \frac{k+1}{n-\alpha\beta+1} P_{n-\alpha\beta+1,k+1}(x)\right].$$

Since the preliminary information on the operator has been presented, the new operator is introduced in the next section.

3. The structure of the new hybrid operator

In this section, inspired by the structure of operators defined in the literature, a new modified double-sum operator will be defined using the λ-parameter.

The use of basis functions in Bernstein-Stancu-type operators is essential for describing the analytical structure and geometric behavior of Bézier-type curves. This approach connects the parametric flexibility of the operators with geometric modeling techniques and provides a useful framework for visual representation. In this context, the analysis of the basis functions supports the interpretation of the corresponding curves and their approximation properties. Therefore, the following definition is introduced as a basis for the subsequent theoretical and application-oriented sections of the study.

Definition 3.1. For $\lambda \in [-1,1]$, $j = 0,1,\dots,\beta$, the λ-modified form of the internal basis functions $P_{\beta,j}(x)$ is denoted by $P_{\beta,j}^{(\lambda)}(x)$ and is given by the following equalities.

For the endpoint indices:

$$P_{\beta,0}^{(\lambda)}(x) = P_{\beta,0}(x) - \lambda \frac{1}{\beta+1} P_{\beta+1,1}(x),$$

$$P_{\beta,\beta}^{(\lambda)}(x) = P_{\beta,\beta}(x) - \lambda \frac{1}{\beta+1} P_{\beta+1,\beta}(x),$$

and for intermediate indices $1 \le j \le \beta - 1$;

$$P_{\beta,j}^{(\lambda)}(x) = P_{\beta,j}(x) + \lambda \left(\frac{\beta - 2j + 1}{\beta^2 - 1} P_{\beta+1,j}(x) - \frac{\beta - 2j - 1}{\beta^2 - 1} P_{\beta+1,j+1}(x) \right).$$

Definition 3.2. For $\lambda \in [-1,1]$, $k = 0,1,\dots,n-\alpha\beta$, the λ-modified form of the external basis function $P_{n-\alpha\beta,k}(x)$ is denoted by $P_{n-\alpha\beta,k}^{(\lambda)}(x)$ and is given as follows.

Endpoint indices:

$$P_{n-\alpha\beta,0}^{(\lambda)}(x) = P_{n-\alpha\beta,0}(x) - \lambda \frac{1}{n-\alpha\beta+1} P_{n-\alpha\beta+1,1}(x),$$

$$P_{n-\alpha\beta,n-\alpha\beta}^{(\lambda)}(x) = P_{n-\alpha\beta,n-\alpha\beta}(x) - \lambda \frac{1}{n-\alpha\beta+1} P_{n-\alpha\beta+1,n-\alpha\beta}(x).$$

For the intermediate indices $1 \le k \le n - \alpha\beta - 1$, the following equality is obtained:

$$P_{n-\alpha\beta,k}^{(\lambda)}(x) = \lambda \left(\frac{n-\alpha\beta-2k+1}{(n-\alpha\beta)^2-1} P_{n-\alpha\beta+1,k}(x) - \frac{n-\alpha\beta-2k-1}{(n-\alpha\beta)^2-1} P_{n-\alpha\beta+1,k+1}(x) \right)$$

$$+P_{n-\alpha\beta,k}(x).$$

The λ-modified basis functions allow us to introduce the following hybrid operator and provide a basis for the application-oriented geometric models considered in this study.

Definition 3.3. Using the definitions of $P_{n-\alpha\beta,k}^{(\lambda)}(x)$ and $P_{\beta,j}^{(\lambda)}(x)$, the two-parameter hybrid operator is defined as follows:

$$N_{n,\alpha,\beta}^{(\lambda)}(f,x) := \left(\frac{n}{n+\beta_2}\right)^{(\alpha-1)\beta-n} \sum_{k=0}^{n-\alpha\beta} P_{n-\alpha\beta,k}^{(\lambda)}(x) \sum_{j=0}^{\beta} P_{\beta,j}^{(\lambda)}(x) f\left(\frac{k+j\alpha_1}{n+\beta_1}\right). \tag{2}$$

For a clearer analysis of the proposed operator, its basis functions are stated explicitly below.

Remark 3.1. If $\lambda = 0$, then $P_{\beta,j}^{(\lambda)}(x) = P_{\beta,j}(x)$ and $P_{n-\alpha\beta,k}^{(\lambda)}(x) = P_{n-\alpha\beta,k}(x)$. Hence, the λ-modified structure reduces to the operator defined in (1).

The positivity and linearity properties, which are essential for the validity of the approximation results, are discussed in detail for this operator.

Theorem 3.1. The operator $N_{n,\alpha,\beta}^{(\lambda)}(f,x)$ is linear and positive.

Proof. Assume that $\frac{\alpha_2}{n+\beta_2} \leq x \leq \frac{n+\alpha_2}{n+\beta_2}$, $0 \leq \alpha_2 \leq \alpha_1 \leq \beta_1 \leq \beta_2$ and $n > \alpha\beta$, for all $\lambda \in [-1,1], j = 0,1,\ldots,\beta$, $k = 0,1,\ldots,n-\alpha\beta$

$$\left(\frac{n}{n+\beta_2}\right)^{(\alpha-1)\beta-n} \geq 0, P_{\beta,j}(x) \geq 0, P_{n-\alpha\beta,k}(x) \geq 0.$$

For the intermediate indices $1 \leq j \leq \beta - 1$, the following equality is obtained:

$$P_{\beta,j}^{(\lambda)}(x) = P_{\beta,j}(x)\left[1 + \frac{\lambda}{\beta-1}\left\{\frac{\beta-2j+1}{\beta+1-j}\left(\frac{n+\alpha_2}{n+\beta_2} - x\right) - \frac{\beta-2j-1}{j+1}\left(x - \frac{\alpha_2}{n+\beta_2}\right)\right\}\right].$$

Since $P_{\beta,j}(x) \geq 0$, it is sufficient to show that the expression in brackets is nonnegative.

$$\frac{\beta-2j+1}{\beta+1-j}\left(\frac{n+\alpha_2}{n+\beta_2} - x\right) - \frac{\beta-2j-1}{j+1}\left(x - \frac{\alpha_2}{n+\beta_2}\right).$$

The expression above is linear in x.

$$\left|\frac{\beta-2j+1}{\beta+1-j}\left(\frac{n}{n+\beta_2}\right)\right| \leq 1 \leq \beta - 1, \text{for } x = \frac{\alpha_2}{n+\beta_2},$$

$$\left|\frac{\beta-2j+1}{(\beta-1)(\beta+1-j)}\left(\frac{n+\alpha_2}{n+\beta_2} - x\right) - \frac{\beta-2j-1}{(\beta-1)(j+1)}\left(x - \frac{\alpha_2}{n+\beta_2}\right)\right| \leq \beta - 1,$$

for

$$x = \frac{n+\alpha_2}{n+\beta_2}.$$

Also, $|\lambda| \leq 1$. Then

$$\left|\frac{\lambda}{\beta-1}\right|\left|\frac{\beta-2j+1}{(\beta-1)(\beta+1-j)}\left(\frac{n+\alpha_2}{n+\beta_2}-x\right)-\frac{\beta-2j-1}{(\beta-1)(j+1)}\left(x-\frac{\alpha_2}{n+\beta_2}\right)\right|\leq 1.$$

So,

$$-1\leq\frac{\lambda}{\beta-1}\left|\frac{\beta-2j+1}{(\beta-1)(\beta+1-j)}\left(\frac{n+\alpha_2}{n+\beta_2}-x\right)-\frac{\beta-2j-1}{(\beta-1)(j+1)}\left(x-\frac{\alpha_2}{n+\beta_2}\right)\right|\leq 1.$$

Therefore, here $P_{\beta,j}^{(\lambda)}(x)\geq 0$.

For the endpoint, since $P_{\beta,0}(x)\geq 0$ and $P_{\beta,\beta}(x)\geq 0$, the required nonnegativity follows directly from the definition.

$$P_{\beta,0}^{(\lambda)}(x)=P_{\beta,0}(x)\left[1-\lambda\frac{1}{\beta+1}\left(x-\frac{\alpha_2}{n+\beta_2}\right)\right].$$

Since $|\lambda|\leq 1$, it follows that $\lambda\left(x-\frac{\alpha_2}{n+\beta_2}\right)\leq 1$ and $0\leq 1-\lambda\left(x-\frac{\alpha_2}{n+\beta_2}\right)$ are obtained. Hence, $P_{\beta,0}^{(\lambda)}(x)\geq 0$.

For the remaining endpoint index $j=\beta$,

$$P_{\beta,\beta}^{(\lambda)}(x)=P_{\beta,\beta}(x)\left[1-\lambda\frac{1}{\beta+1}\left(\frac{n+\alpha_2}{n+\beta_2}-x\right)\right]$$

is obtained. Using $|\lambda|\leq 1$, $\lambda\left(\frac{n+\alpha_2}{n+\beta_2}-x\right)\leq 1$ and $0\leq 1-\lambda\left(\frac{n+\alpha_2}{n+\beta_2}-x\right)$. It follows that, $P_{\beta,\beta}^{(\lambda)}(x)\geq 0$. The nonnegativity of the remaining basis functions follows similarly.

Remark 3.3. If $\lambda=0$, then $N_{n,\alpha,\beta}^{(\lambda)}(f,x)=N_{n,\alpha,\beta}(f,x)$.

To apply Korovkin's theorem, the action of the operator on the test functions is examined.

Notation 3.1. For clarity of presentation, the following notation is adopted in the subsequent analysis.

$$\frac{n}{n+\beta_2}:=\xi, x-\frac{\alpha_2}{n+\beta_2}:=\kappa, n-\alpha\beta:=\varrho, \frac{1}{n+\beta_1}:=\varsigma,$$

$$M(\varrho):=\frac{\{\kappa\varrho\xi+\kappa^2\varrho(\varrho-1)\}\varsigma^2}{\xi^2},$$

$$H(\varrho):=\frac{\kappa\varrho}{\xi}-\frac{\lambda[(\xi-\kappa)^{\varrho+1}+\kappa^{\varrho+1}-\xi^{\varrho+1}+2\kappa\xi^{\varrho}]}{(\varrho-1)\xi^{\varrho}},$$

$$G(\varrho):=\frac{\kappa\varrho(\varrho-1)\xi^{\varrho-1}-\lambda\{(\xi-\kappa)^{\varrho+1}+\kappa^{\varrho+1}-\xi^{\varrho+1}+2\kappa\xi^{\varrho}\}}{(\varrho-1)\xi^{\varrho}}.$$

Lemma 3.1. For the operator defined by (2), the following equalities hold:

$(i)\ N_{n,\alpha,\beta}^{(\lambda)}(1,x)=1,$

$(ii)\ N_{n,\alpha,\beta}^{(\lambda)}(t,x)=\varsigma[H(\varrho)+\alpha_1 H(\beta)],$

$$(iii)N_{n,\alpha,\beta}^{(\lambda)}(t^2,x)=\frac{\lambda\varsigma^2}{\xi\varrho}\sum_{k=1}^{\varrho}\frac{(2k-1)(\varrho-2k+1)}{\varrho^2-1}P_{\varrho+1,k}(x)+2\alpha_1\varsigma^2G(\varrho)G(\beta)$$
$$+\alpha_1{}^2\varsigma^2\left[M(\beta)+\lambda\sum_{j=1}^{\beta}\frac{(2j-1)(\beta-2j+1)}{\beta^2-1}P_{\beta+1,j}(x)\right]+M(\varrho).$$

To examine the convergence properties of the proposed operator, its limiting behavior on the test functions used in the Korovkin-type approximation theorem is considered.

Lemma 3.2. For the operator $N_{n,\alpha,\beta}^{(\lambda)}(t,x)$, the following limits hold:

$(i)\ \lim\limits_{n\to\infty} N_{n,\alpha,\beta}^{(\lambda)}(1,x)=1,$

$(ii)\ \lim\limits_{n\to\infty} N_{n,\alpha,\beta}^{(\lambda)}(t,x)=x,$

$(ii)\ \lim\limits_{n\to\infty} N_{n,\alpha,\beta}^{(\lambda)}(t^2,x)=x^2.$

The following Korovkin-type theorem states that every continuous function on the considered space can be uniformly approximated by the proposed operator.

Theorem 3.2. For $x\in\left[\frac{\alpha_2}{n+\beta_2},\frac{n+\alpha_2}{n+\beta_2}\right],\ 0\le\alpha_2\le\alpha_1\le\beta_1\le\beta_2, n>\alpha\beta$ and for all $f\in C\left[\frac{\alpha_2}{n+\beta_2},\frac{n+\alpha_2}{n+\beta_2}\right]$,

$$\lim_{n\to\infty}\left\|N_{n,\alpha,\beta}^{(\lambda)}(f,x)-f(x)\right\|_{C\left[\frac{\alpha_2}{n+\beta_2},\frac{n+\alpha_2}{n+\beta_2}\right]}=0.$$

The proof follows directly from Lemmas 3.1 and 3.2.

Following the approximation theorem, error estimation is an important component in evaluating the effectiveness of the proposed operator. The main purpose of the operator is to approximate a given function with respect to specific parameters. However, the reliability of this process depends on determining appropriate error bounds for the resulting approximation. Through error analysis, the rates of convergence and degrees of accuracy of the operators can be examined, thereby supporting the transfer of theoretical results to practical applications. In particular, the flexibility of the parametric structure enables more effective error estimation for different classes of functions. Therefore, in this study on DD Stancu operators, error estimation is viewed not only as a technical detail but also a fundamental criterion for demonstrating the effectiveness and mathematical value of the operator.

Error estimates are obtained using the modulus of continuity to determine the rate of convergence of the operator.

Figure 1 illustrates how various error metrics (maximum error, mean error, and RMS error) change as the parameter λ varies. A vertical dashed line indicates the λ value that yields the minimum maximum error, representing the optimal λ found through the search.

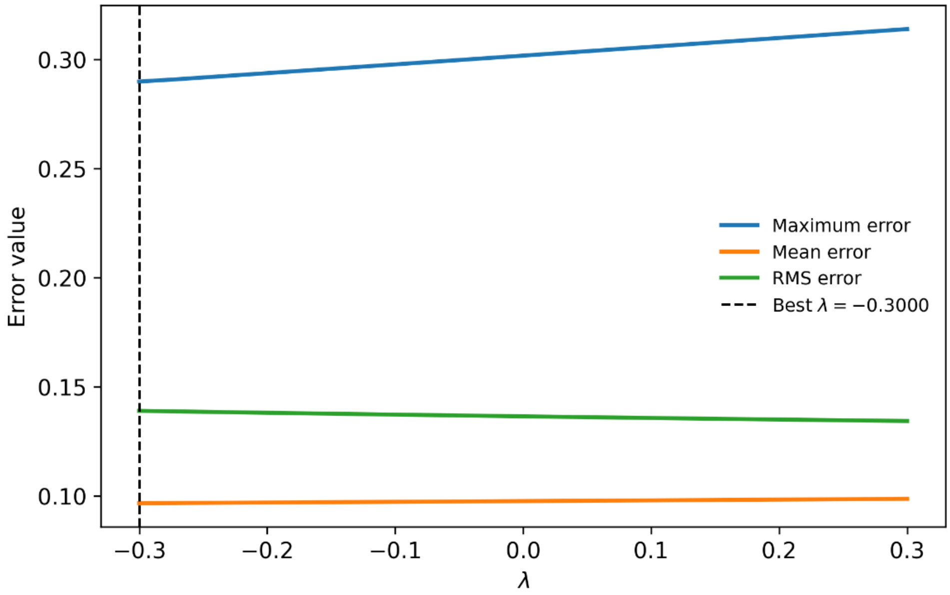

Figure 1. Error metrics with respect to λ.

In Figure 2, the exact function $f(x)$ is compared with two approximations: the classical case ($\lambda = 0$) and the approximation using the optimal λ identified in Figure 1. It demonstrates the improvement in approximation accuracy achieved with the optimized λ value.

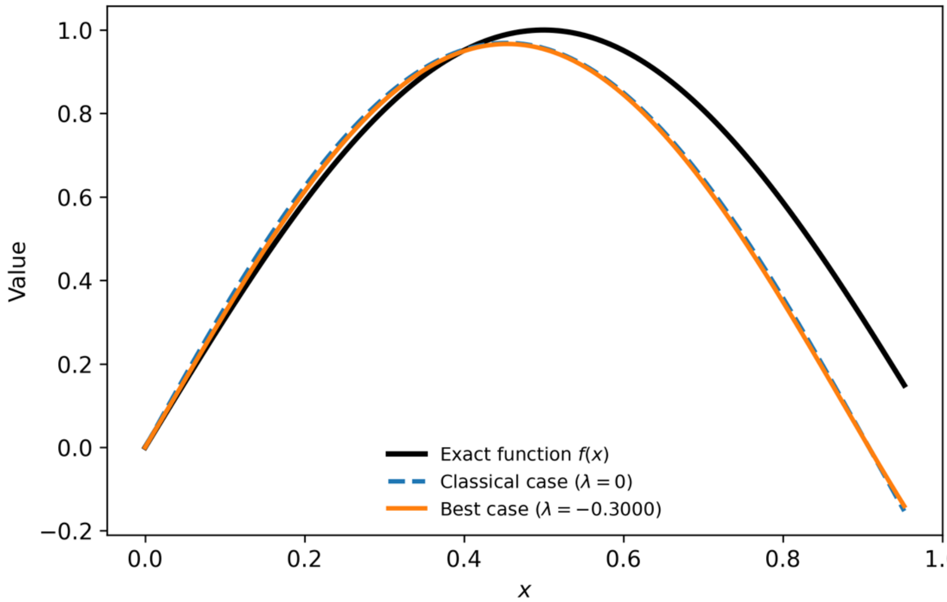

Figure 2. Classical approximation and optimal λ-approximation.

Figure 3 compares the absolute error curves for the classical approximation $\lambda = 0$ and the approximation using the optimal λ value. It highlights the regions where the approximation obtained with the optimal λ value reduces the error compared with the classical case, providing a clearer understanding of the benefits of optimization.

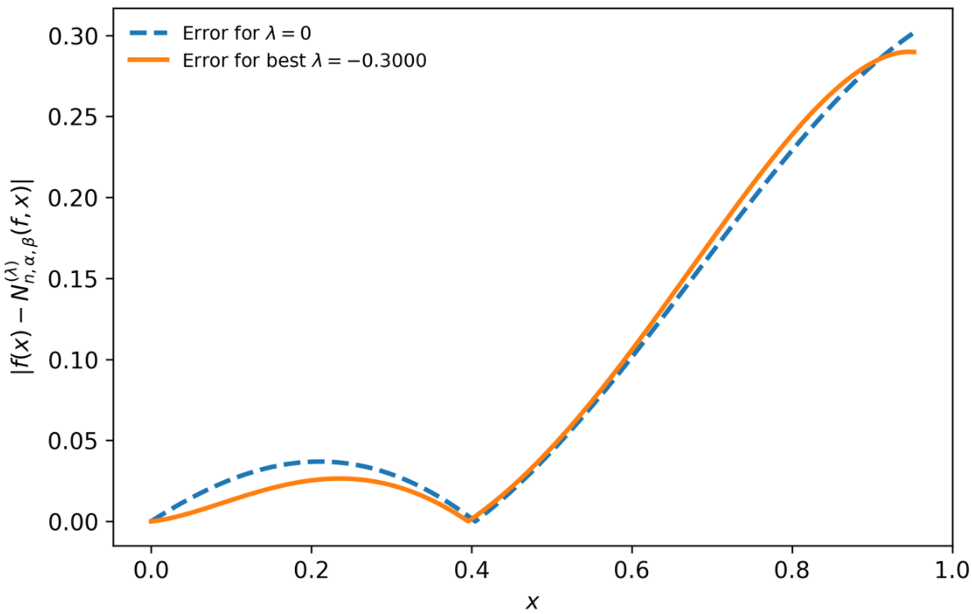

Figure 3. Error comparison: Classical case vs optimal λ.

Figure 4 shows that changes in the λ parameter directly affect the approximation behavior of the operator; specifically, positive λ values provide a closer approximation to the reference profile, whereas negative λ values lead to larger deviations from the curve.

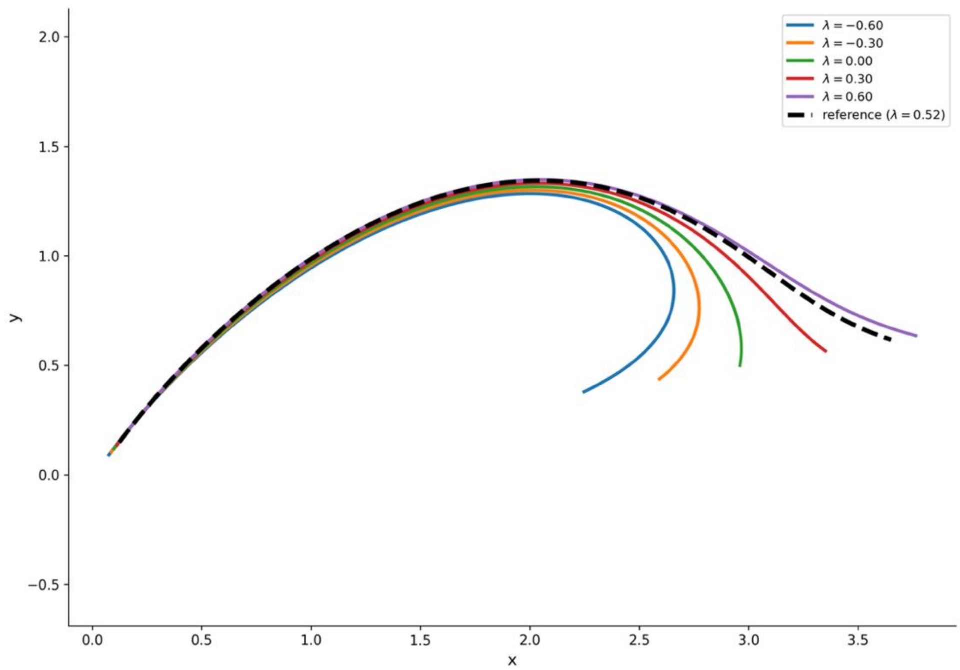

Figure 4. Operator approximation to the curve for several λ values.

Figure 5 illustrates the approximation of the exact function $f(x) = \sin(\pi x)$ by the λ-modified operator $N_{n,\alpha,\beta}^{(\lambda)}(f,x)$ for different values of n. As the parameter n increases, the approximation generally improves, demonstrating the convergence of the operator to the exact function.

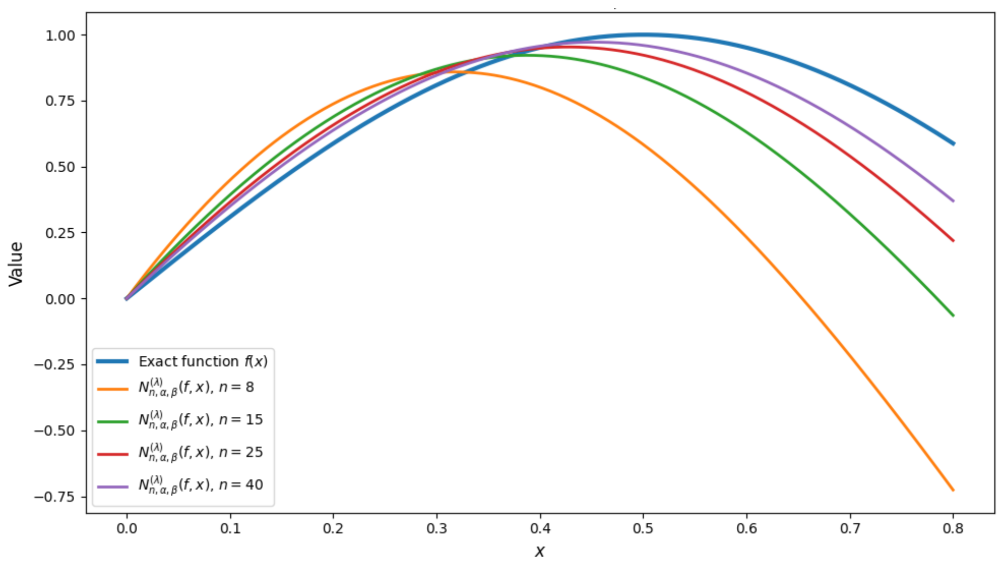

Figure 5. Approximation by the λ-modified operator.

Figure 6 presents the absolute error between the exact function and its approximation by the λ-modified operator for various values of n. The figure illustrates that larger values of n lead to smaller approximation errors, indicating improved accuracy of the operator.

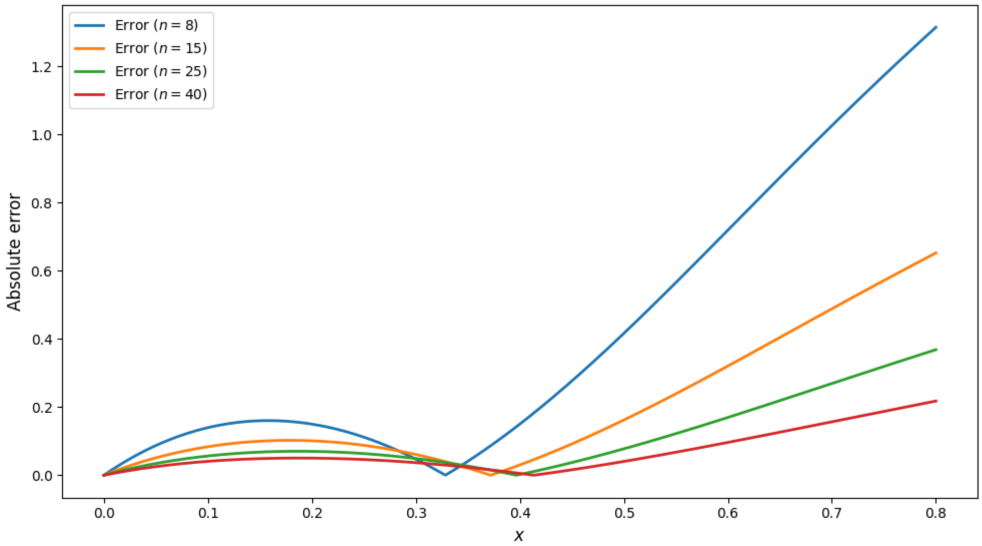

Figure 6. Error analysis of approximation.

For the considered function f, the approximation behaviors of the classical-type first operator given by Eq (7) in [30] and the proposed hybrid operator are compared in terms of the maximum absolute error in Figures 7 and 8. The numerical results show that, under suitable choices of the parameters $\lambda, \alpha_1, \alpha_2, \beta_1, \beta_2, \alpha$, and β, the proposed hybrid operator approximates the target function with a smaller error than the first operator. This improvement can be attributed to the double-sum structure of the new operator, which consists of inner and outer basis functions and allows a more flexible distribution of weights. In particular, the additional parameters α and β provides an extra degree of adjustment, enabling a more accurate approximation for certain classes of functions. However, this superiority should not be interpreted as a universal result for all parameter values and all functions. The performance of the new operator depends on the selected parameters, the admissibility condition $(n - \alpha\beta > 1)$, and the behavior of the target function. Therefore, the main advantage of the proposed operator is its ability to yield better approximation results under appropriate parameter choices and its flexible structure, whereas its main limitation is that the observed improvement is parameter-and function-dependent rather than general. Consequently, the numerical findings indicate that the new operator can serve as a more effective approximation tool than the first operator, provided that the parameters are chosen carefully to achieve optimal performance.

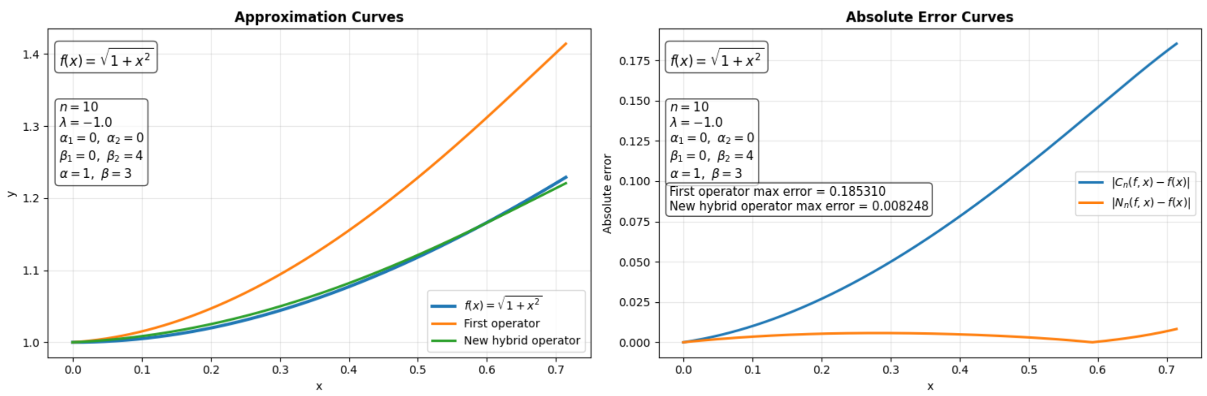

Figure 7. Approximation comparison for $f(x)=\sqrt{1+x^2}$.

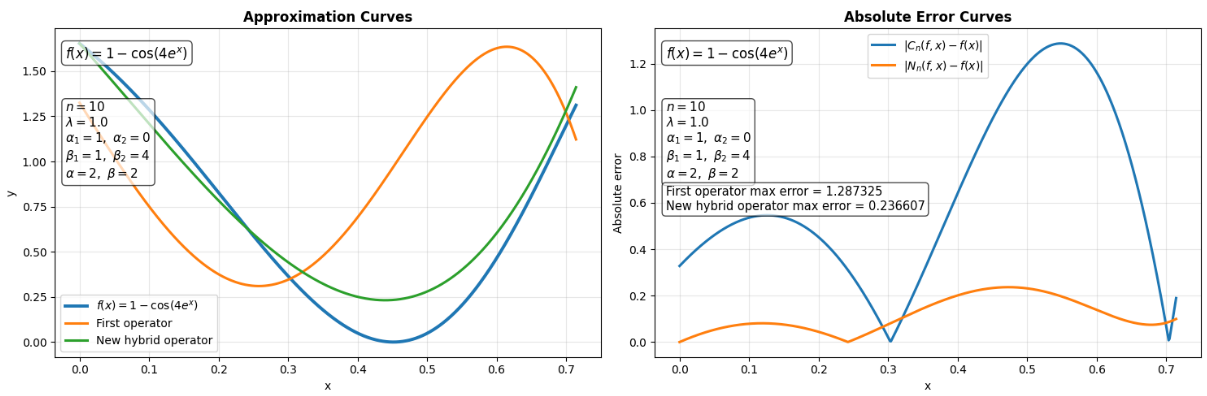

Figure 8. Approximation comparison for $f(x)=1-\cos(4e^x)$.

The modulus of continuity provides a fundamental framework for determining the rate of convergence and evaluating the approximation behavior of the operator in the theoretical setting of this study.

Theorem 3.3. For $x\in\left[\frac{\alpha_2}{n+\beta_2},\frac{n+\alpha_2}{n+\beta_2}\right]$, $0\le\alpha_2\le\alpha_1\le\beta_1\le\beta_2$ and $n>\alpha\beta$, then, for sufficiently large n,

$$\left|N_{n,\alpha,\beta}^{(\lambda)}(f,x)-f(x)\right|\le 2\,\omega\left(f,\sqrt{N_{n,\alpha,\beta}^{(\lambda)}((t-x)^2;x)}\right).$$

Proof. Since $N_{n,\alpha,\beta}^{(\lambda)}((t-x)^2;x)\le\frac{K}{n}$, for a suitable constant $K>0$, it follows that

$$\left|N_{n,\alpha,\beta}^{(\lambda)}(f;x)-f(x)\right|\le 2\omega\left(f,\frac{C}{\sqrt{n}}\right),$$

where $C>0$ is a suitable constant. Taking

$$K:=M_2+2(1+\alpha_2)M_1,$$

$$M_1:=[|\beta_2-\beta_1-\alpha\beta|+\alpha\beta\beta_2](1+\alpha_2)+(1+\beta_2)\alpha_2+\alpha_1\beta(1+\alpha_2)+|\lambda|\left(2e^{\beta_2}+3\right)$$

$$+\frac{|\lambda|\alpha_1}{(\beta-1)}\big(2(1+\beta_2)^{\beta}+3\big),$$

$$M_2 \coloneqq (1+\beta_2)+\big(2\alpha\beta+1+2\beta_1+\alpha\beta(\alpha\beta+1)+{\beta_1}^2\big)(1+\beta_2)^2+2\beta_2+\beta_2^2$$

$$+2(1+\alpha_2)\alpha_2+\alpha_2^2+2|\lambda|e^{\beta_2}+\frac{{\alpha_1}^2}{n}[\beta(1+\beta_2)+\beta(\beta-1)(1+\beta_2)^2+4\beta|\lambda|]$$

$$+2\alpha_1\big[(1+\beta_2)n+|\lambda|\big(2e^{\beta_2}+3\big)\big]\left[\beta(1+\beta_2)+\frac{|\lambda|}{\beta-1}\big(2(n+\beta_2)^{\beta}+3\big)\right].$$

Therefore, the desired inequality follows by standard algebraic computations.

The Lipschitz-type approximation provides a useful framework for evaluating the convergence behavior of the proposed DD Stancu-type operator. Since the Lipschitz condition is a standard tool for measuring the smoothness of functions, it allows error estimates to be expressed in terms of the regularity of the approximated function. Moreover, the analysis of functions in Lipschitz classes helps clarify how the operator behaves under different parameter choices. Therefore, the Lipschitz-type approximation is considered a complementary part of the theoretical analysis of the proposed Bernstein-Stancu-type operator.

The convergence theorem for functions in Lipschitz classes is given below.

Theorem 3.4. For every $x\in\left[\frac{\alpha_2}{n+\beta_2},\frac{n+\alpha_2}{n+\beta_2}\right]$ and for $f\in Lip(\gamma), 0<\gamma<1$, there exists a constant $M>0$ such that

$$\left|N_{n,\alpha,\beta}^{(\lambda)}(f;x)-f(x)\right|\le M\left(\frac{K}{n}\right)^{\frac{\gamma}{2}}.$$

The proof follows from Lemmas 3.1 and 3.2.

The following relation for the λ-modified basis functions is useful in explaining the analytic structure of the operator.

Theorem 3.5. For all $x\in\left[\frac{\alpha_2}{n+\beta_2},\frac{n+\alpha_2}{n+\beta_2}\right]$ and $\lambda\in[-1,1]$, the following properties hold.

(i) For the boundary case $k=0$,

$$P_{n-\alpha\beta,k}^{(\lambda)}(x)=\left(\frac{n+\beta_2}{n}\right)P_{n-\alpha\beta+1,0}(x)+\frac{P_{n-\alpha\beta+1,1}(x)}{n-\alpha\beta+1}\left(\left(\frac{n+\beta_2}{n}\right)-\lambda\right).$$

(ii) For the interior case $1\le k\le n-\alpha\beta-1$,

$$P_{n-\alpha\beta,k}^{(\lambda)}(x)=\left[\left(\frac{n+\beta_2}{n}\right)\frac{n-\alpha\beta+1-k}{n-\alpha\beta+1}+\lambda\frac{n-\alpha\beta-2k+1}{(n-\alpha\beta)^2-1}\right]P_{n-\alpha\beta+1,k}(x)$$

$$+\left[\left(\frac{n+\beta_2}{n}\right)\frac{k+1}{n-\alpha\beta+1}-\frac{n-\alpha\beta-2k-1}{(n-\alpha\beta)^2-1}\right]P_{n-\alpha\beta+1,k+1}(x).$$

(iii) For the boundary case $k = n - \alpha\beta$,

$$P_{n-\alpha\beta,n-\alpha\beta}^{(\lambda)}(x) = \left(\frac{n+\beta_2}{n}\right) P_{n-\alpha\beta+1,n-\alpha\beta+1}(x) + \frac{P_{n-\alpha\beta+1,n-\alpha\beta}(x)}{n-\alpha\beta+1}\left(\left(\frac{n+\beta_2}{n}\right) - \lambda\right).$$

Proposition 3.1. For all $x \in \left[\frac{\alpha_2}{n+\beta_2}, \frac{n+\alpha_2}{n+\beta_2}\right]$ and $\lambda \in [-1,1]$, $P_{\beta,j}^{(\lambda)}(x) \geq 0$ and $P_{n-\alpha\beta,k}^{(\lambda)}(x) \geq 0$.

The λ -modified basis functions satisfy a specific symmetry property, which is stated in the following lemma.

Lemma 3.6. The following equalities hold:

(i) $P_{\beta,j}^{(\lambda)}(x) = P_{\beta,\beta-j}^{(\lambda)}\left(\frac{n+2\alpha_2}{n+\beta_2} - x\right)$, for $j = 0,1,\dots,\beta$.

(ii) $P_{n-\alpha\beta,k}^{(\lambda)}(x) = P_{n-\alpha\beta,n-\alpha\beta-k}^{(\lambda)}\left(\frac{n+2\alpha_2}{n+\beta_2} - x\right)$, for $k = 0,1,\dots n - \alpha\beta$.

The linear independence of the basis functions is established in the following lemma.

Lemma 3.7. The following properties are satisfied:

(i) $\sum_{j=0}^{\beta} c_j P_{\beta,j}^{(\lambda)}(x) = 0 \Leftrightarrow c_j = 0,$

(ii) $\sum_{k=0}^{n-\alpha\beta} d_k P_{n-\alpha\beta,k}^{(\lambda)}(x) = 0 \Leftrightarrow d_k = 0.$

Proof. (i) For each $x \in \left[\frac{\alpha_2}{n+\beta_2}, \frac{n+\alpha_2}{n+\beta_2}\right]$ and $\lambda \in [-1,1]$. Using the endpoints $x_0 = \frac{\alpha_2}{n+\beta_2}, x_1 = \frac{n+\alpha_2}{n+\beta_2}$. At the left endpoint $x = x_0$, the endpoint property of the basis functions gives $P_{\beta,0}^{(\lambda)}(x_0) > 0$, $P_{\beta,j}^{(\lambda)}(x_0) = 0$, $j = 1,\dots,\beta$.

Here, $c_0 P_{\beta,0}^{(\lambda)}(x_0) = 0$, then $c_0 = 0$ is obtained. When $x = x_1$, for $j = 0,1,\dots,\beta - 1$, then $P_{\beta,\beta}^{(\lambda)}(x_1) > 0$, $P_{\beta,j}^{(\lambda)}(x_1) = 0$, therefore, $c_\beta = 0$ is obtained.

After taking the i-th derivative of both sides and setting $x = x_0$, the following equality is obtained:

$$\sum_{j=0}^{\beta} c_j \left(P_{\beta,j}^{(\lambda)}\right)^{(i)}(x) = 0, \qquad j = 1,\dots,\beta - 1.$$

Then, $P_{\beta,j}^{(\lambda)}(x)$ contains at least one factor $(x - x_0)^j$. If $j > i$, then $\left(P_{\beta,j}^{(\lambda)}\right)^{(i)}(x_0) = 0$, and also

$\left(P_{\beta,i}^{(\lambda)}\right)^{(i)}(x_0) > 0$. Therefore, the coefficients $c_0, c_1, \dots, c_{i-1}$ have already been shown to be zero. Upon setting $x = x_0$, only the term with $j = i$ remains. Thus,

$$c_i\left(P_{\beta,i}^{(\lambda)}\right)^{(i)}(x_0) = 0. \text{Since } \left(P_{\beta,i}^{(\lambda)}\right)^{(i)}(x_0) > 0, c_i = 0, \qquad j = 1, \dots, \beta - 1.$$

Consequently,

$$c_0 = c_1 = \cdots = c_\beta = 0.$$

This completes the proof of (i).

The proof of (ii) is obtained by a similar technique.

The integral formulas involving the basis functions of the operator defined in (2) are given below.

Lemma 3.8. The following properties are obtained:

(i) $\displaystyle\int_{x_0}^{x_1} P_{\beta,j}(x)dx = \left(\frac{n}{n+\beta_2}\right)^{\beta+1}\frac{1}{\beta+1}$,

(ii) For all $j = 0,1, \dots, \beta + 1$

$$\int_{x_0}^{x_1} P_{\beta+1,j}(x)dx = \left(\frac{n}{n+\beta_2}\right)^{\beta+2}\frac{1}{\beta+2}.$$

The integral properties of λ-modified basis functions are given below:

Proposition 3.2. For $\lambda \in [-1,1]$ and $x_0 = \frac{\alpha_2}{n+\beta_2}, x_1 = \frac{n+\alpha_2}{n+\beta_2}$, the following identities hold:

$$\int_{x_0}^{x_1} P_{\beta,0}^{(\lambda)}(x)dx = \left(\frac{n}{n+\beta_2}\right)^{\beta+1}\frac{1}{\beta+1} - \lambda\frac{1}{\beta+1}\left(\frac{n}{n+\beta_2}\right)^{\beta+2}\frac{1}{\beta+2},$$

$$\int_{x_0}^{x_1} P_{\beta,\beta}^{(\lambda)}(x)dx = \left(\frac{n}{n+\beta_2}\right)^{\beta+1}\frac{1}{\beta+1} - \lambda\frac{1}{\beta+1}\left(\frac{n}{n+\beta_2}\right)^{\beta+2}\frac{1}{\beta+2},$$

for intermediate indices $1 \le j \le \beta - 1$;

$$\int_{x_0}^{x_1} P_{\beta,j}^{(\lambda)}(x)dx = \left(\frac{n}{n+\beta_2}\right)^{\beta+1}\frac{1}{\beta+1} + \frac{2\lambda}{\beta^2-1}\left(\frac{n}{n+\beta_2}\right)^{\beta+2}\frac{1}{\beta+2}.$$

The proof follows directly from Lemma 3.9 and the definitions of the λ-modified basis functions for the boundary and intermediate cases.

Proposition 3.3. For $x_0 = \frac{\alpha_2}{n+\beta_2}$ and $x_1 = \frac{n+\alpha_2}{n+\beta_2}$, $\lambda \in [-1,1]$, the following identities hold:

$$\int_{x_0}^{x_1} P_{n-\alpha\beta,0}^{(\lambda)}(x)dx = \frac{1}{n-\alpha\beta+1}\left(\frac{n}{n+\beta_2}\right)^{n-\alpha\beta+1}\left[1-\frac{n\lambda}{(n+\beta_2)(n-\alpha\beta+2)}\right],$$

$$\int_{x_0}^{x_1} P_{n-\alpha\beta,n-\alpha\beta}^{(\lambda)}(x)dx = \frac{1}{n-\alpha\beta+1}\left(\frac{n}{n+\beta_2}\right)^{n-\alpha\beta+1}\left[1-\frac{n\lambda}{(n+\beta_2)(n-\alpha\beta+2)}\right],$$

intermediate indices $1 \leq k \leq n-\alpha\beta-1$,

$$\int_{x_0}^{x_1} P_{n-\alpha\beta,k}^{(\lambda)}(x)dx = \left(\frac{n}{n+\beta_2}\right)^{n-\alpha\beta+1}\left[\frac{2n\lambda}{((n-\alpha\beta)^2-1)(n+\beta_2)(n-\alpha\beta+2)(n-\alpha\beta+1)}\right.$$
$$\left.+\frac{1}{n-\alpha\beta+1}\right].$$

Within the structural analysis of the basis functions, their unimodality properties are examined in detail using a method similar to that described in [25].

The unimodality argument used in this theorem is inspired by the approach of Ye et al. [25], who proved the unimodality of lambda-modified Bernstein basis functions through their Bézier curve representation and the variation-diminishing property. In the present study, this idea is adapted to the product-type basis function arising from the double-sum structure of the proposed hybrid DD Stancu operator. Thus, the contribution here is not the introduction of a completely new unimodality principle, but rather the verification that this property is preserved under the lambda-modified product basis structure of the proposed operator.

Lemma 3.9. For fixed indices $j = 0,1,\dots,\beta$ and $k = 0,1,\dots,n-\alpha\beta$, the λ-modified product basis function $\varphi_{k,j}^{(\lambda)}(x)$ is unimodal on the interval $\left[\frac{\alpha_2}{n+\beta_2},\frac{n+\alpha_2}{n+\beta_2}\right]$.

$$\varphi_{k,j}^{(\lambda)}(x) = P_{\beta,j}^{(\lambda)}(x).P_{n-\alpha\beta,k}^{(\lambda)}(x).$$

Proof. For $n \geq 2$ and $j = 0,1,\dots,\beta$, the λ-modified basis function is written as

$$P_{\beta,j}^{(\lambda)}(x) = P_{\beta,j}(x) + \lambda\left(\frac{\beta-2j+1}{\beta^2-1}P_{\beta+1,j}(x) - \frac{\beta-2j-1}{\beta^2-1}P_{\beta+1,j+1}(x)\right).$$

First, it is shown that $P_{\beta,j}^{(\lambda)}(x)$ is unimodal.

From the definition of $P_{\beta,j}(x)$, the following relations are obtained:

$$P_{\beta+1,j}(x) = \frac{\beta+1}{\beta+1-j}\left(\frac{n+\alpha_2}{n+\beta_2}-x\right)P_{\beta,j}(x)$$

and

$$P_{\beta+1,j+1}(x)=\frac{\beta+1}{j+1}\left(x-\frac{\alpha_2}{n+\beta_2}\right)P_{\beta,j}(x).$$

Substituting these relations into $P_{\beta,j}^{(\lambda)}(x)$ gives

$$P_{\beta,j}^{(\lambda)}(x)=P_{\beta,j}(x)\{1+\lambda\left[\frac{\beta-2j+1}{(\beta-1)(\beta+1-j)}\frac{n+\alpha_2}{n+\beta_2}+\frac{\beta-2j-1}{(\beta-1)(j+1)}\frac{\alpha_2}{n+\beta_2}\right.$$
$$\left.-\left\{\frac{\beta-2j+1}{(\beta-1)(\beta+1-j)}+\frac{\beta-2j-1}{(\beta-1)(j+1)}\right\}x\right].$$

Using the positivity of $P_{\beta,j}^{(\lambda)}(x)$, taking logarithms yields

$$ln\left\{P_{\beta,j}^{(\lambda)}(x)\right\}=lnP_{\beta,j}(x)+ln\{1+\lambda\left[\frac{\beta-2j+1}{(\beta-1)(\beta+1-j)}\frac{n+\alpha_2}{n+\beta_2}+\frac{\beta-2j-1}{(\beta-1)(j+1)}\frac{\alpha_2}{n+\beta_2}\right.$$
$$\left.-\left\{\frac{\beta-2j+1}{(\beta-1)(\beta+1-j)}+\frac{\beta-2j-1}{(\beta-1)(j+1)}\right\}x\right].$$

The derivative of $\left\{lnP_{\beta,j}(x)\right\}$ is decreasing, since

$$\left\{lnP_{\beta,j}(x)\right\}'=j\left(x-\tfrac{\alpha_2}{n+\beta_2}\right)^{-1}-(\beta-j)\left(\tfrac{n+\alpha_2}{n+\beta_2}-x\right)^{-1},$$

$$\left\{lnP_{\beta,j}(x)\right\}''=-j\left(x-\tfrac{\alpha_2}{n+\beta_2}\right)^{-2}-(\beta-j)\left(\tfrac{n+\alpha_2}{n+\beta_2}-x\right)^{-2}<0.$$

On the other hand, the second factor in the representation of $P_{\beta,j}^{(\lambda)}(x)$ is denoted by $M(x)$. Then,

$$ln[M(x)]=ln\{1+\lambda\left[\frac{\beta-2j+1}{(\beta-1)(\beta+1-j)}\frac{n+\alpha_2}{n+\beta_2}+\frac{\beta-2j-1}{(\beta-1)(j+1)}\frac{\alpha_2}{n+\beta_2}\right.$$
$$\left.-\left\{\frac{\beta-2j+1}{(\beta-1)(\beta+1-j)}+\frac{\beta-2j-1}{(\beta-1)(j+1)}\right\}x\right],$$

$$\{ln[M(x)]\}'=\frac{-\lambda\left\{\frac{\beta-2j+1}{(\beta-1)(\beta+1-j)}+\frac{\beta-2j-1}{(\beta-1)(j+1)}\right\}}{M(x)},$$

$$\{ln[M(x)]\}''=-\lambda^2\left\{\frac{\beta-2j+1}{(\beta-1)(\beta+1-j)}+\frac{\beta-2j-1}{(\beta-1)(j+1)}\right\}^2[M(x)]^2\leq 0.$$

Since $\{ln[M(x)]\}''\leq 0$, the derivative $\{ln[M(x)]\}'$ is decreasing. Since both $\left[lnP_{\beta,j}^{(\lambda)}(x)\right]'$ and

$\{ln[M(x)]\}'$ are non-increasing, it follows that $\frac{d}{dx} lnP_{\beta,j}^{(\lambda)}(x)$ is non-increasing. Moreover,

$$\frac{d}{dx} lnP_{\beta,j}^{(\lambda)}(x) = \frac{\left[P_{\beta,j}^{(\lambda)}(x)\right]'}{P_{\beta,j}^{(\lambda)}(x)}.$$

Since this logarithmic derivative is non-increasing, it can vanish at most once. Therefore, $\left[P_{\beta,j}^{(\lambda)}(x)\right]'$can change sign at most once, which implies the unimodality of $P_{\beta,j}^{(\lambda)}(x)$. By the same argument, the unimodality of $P_{n-\alpha\beta,k}^{(\lambda)}(x)$ follows.

Thus, for the product basis function $\varphi_{k,j}^{(\lambda)}(x)$, the logarithmic representation is given by

$$ln\varphi_{k,j}^{(\lambda)}(x) = lnP_{\beta,j}^{(\lambda)}(x) + lnP_{n-\alpha\beta,k}^{(\lambda)}(x).$$

By differentiating both sides, the following equality is obtained:

$$\left\{ln\varphi_{k,j}^{(\lambda)}(x)\right\}' = \left\{lnP_{\beta,j}^{(\lambda)}(x)\right\}' + \left\{lnP_{n-\alpha\beta,k}^{(\lambda)}(x)\right\}'.$$

Since the right-hand side is the sum of two non-decreasing logarithmic derivatives, it is also non-decreasing. Therefore, $\left\{ln\varphi_{k,j}^{(\lambda)}(x)\right\}'$is non-increasing.

Since $\varphi_{k,j}^{(\lambda)}(x) > 0$, the zeros of $\left\{\varphi_{k,j}^{(\lambda)}(x)\right\}'$ coincide with those of its logarithmic derivative. As this logarithmic derivative is non-increasing, it can change sign at most once. Hence, $\left\{\varphi_{k,j}^{(\lambda)}(x)\right\}'$ can change sign at most once, which implies that the unimodality of $\varphi_{k,j}^{(\lambda)}(x)$ is obtained. This completes the proof.

The λ-modified basis functions satisfy the partition of unity property, which is stated in the following lemma.

Lemma 3.10. For every $x \in \left[\frac{\alpha_2}{n+\beta_2}, \frac{n+\alpha_2}{n+\beta_2}\right]$,

$$\left(\frac{n}{n+\beta_2}\right)^{(\alpha-1)\beta-n} \sum_{k=0}^{n-\alpha\beta} P_{n-\alpha\beta,k}^{(\lambda)}(x) \sum_{j=0}^{\beta} P_{\beta,j}^{(\lambda)}(x) = 1.$$

Proof.

$$K := \left(\frac{n}{n+\beta_2}\right)^{-\beta} \sum_{j=0}^{\beta} P_{\beta,j}^{(\lambda)}(x),$$

$$L := \left(\frac{n}{n+\beta_2}\right)^{\alpha\beta-n} \sum_{k=0}^{n-\alpha\beta} P_{n-\alpha\beta,k}^{(\lambda)}(x).$$

The left-hand side is divided into two factors K and L. It suffices to show that $K \cdot L = 1$.

$$K = \left(\frac{n}{n+\beta_2}\right)^{-\beta} \left\{\left(\frac{n}{n+\beta_2}\right)^{\beta} - \lambda \frac{1}{\beta+1} P_{\beta+1,1}(x) - \lambda \frac{1}{\beta+1} P_{\beta+1,\beta}(x) \right.$$
$$\left. +\lambda \sum_{j=1}^{\beta-1} \left(\frac{\beta-2j+1}{\beta^2-1} P_{\beta+1,j}(x) - \frac{\beta-2j-1}{\beta^2-1} P_{\beta+1,j+1}(x)\right)\right\}.$$

The remaining terms cancel as follows:

$$\lambda \sum_{j=1}^{\beta-2} \frac{\beta-2(j+1)+1}{\beta^2-1} P_{\beta+1,j+1}(x) - \lambda \sum_{j=1}^{\beta-2} \frac{\beta-2j-1}{\beta^2-1} P_{\beta+1,j+1}(x) = 0.$$

By applying the same cancellation argument to L, $L = 1$. Since $K = 1$ as well, it follows that $K \cdot L = 1$. This completes the proof.

A new Bézier-type curve associated with the operator $N_{n,\alpha,\beta}^{(\lambda)}(f,x)$ is introduced in the following definition.

Definition 3.4. For $\psi_{k,j} = f\left(\frac{k+j\alpha_1}{n+\beta_1}\right)$, $j = 0,1,\ldots,\beta$ and $k = 0,1,\ldots,n-\alpha\beta$ and for $\lambda \in [-1,1]$, let $P_{\beta,j}^{(\lambda)}(x)$ and $P_{n-\alpha\beta,k}^{(\lambda)}(x)$ denote the λ-modified basis functions. The λ-modified double-sum Bézier-type curve is defined by

$$\mathfrak{B}_{n,\alpha,\beta}^{(\lambda)}(x) := \left(\frac{n}{n+\beta_2}\right)^{(\alpha-1)\beta-n} \sum_{k=0}^{n-\alpha\beta} P_{n-\alpha\beta,k}^{(\lambda)}(x) \sum_{j=0}^{\beta} P_{\beta,j}^{(\lambda)}(x)\psi_{k,j},$$

where $\frac{\alpha_2}{n+\beta_2} \le x \le \frac{n+\alpha_2}{n+\beta_2}$.

The endpoint interpolation property of the defined Bézier-type curve is stated in the following lemma.

Lemma 3.11. Let $P_{\beta,j}(x), j = 0,1,\ldots,\beta$, denote the λ-modified internal basis functions for $\lambda \in [-1,1]$. Then, the endpoints of the curve $\mathfrak{B}_{n,\alpha,\beta}^{(\lambda)}(x)$ satisfy

$$\mathfrak{B}_{n,\alpha,\beta}^{(\lambda)}\left(\frac{\alpha_2}{n+\beta_2}\right) = \psi_{0,0} \text{ and } \mathfrak{B}_{n,\alpha,\beta}^{(\lambda)}\left(\frac{n+\alpha_2}{n+\beta_2}\right) = \psi_{n-\alpha\beta,\beta}.$$

The derivative values at the endpoints of a Bézier-type curve determine the direction of the tangents at the starting and ending points.

Theorem 3.6. For the λ-modified double-sum Bézier-type curve, the first derivatives at the endpoints are given as follows:

$$(i)\frac{d}{dx}\mathfrak{B}_{n,\alpha,\beta}^{(\lambda)}\left(\frac{\alpha_2}{n+\beta_2}\right)=\left(\frac{n+\beta_2}{n}\right)\left\{\left[n-\alpha\beta+\lambda\frac{n}{n+\beta_2}\right]\left(\psi_{1,0}-\psi_{0,0}\right)\right.$$

$$\left.+\left[\beta+\lambda\frac{n}{n+\beta_2}\right]\left(\psi_{0,1}-\psi_{0,0}\right)\right\},$$

$$(ii)\ \frac{d}{dx}\mathfrak{B}_{n,\alpha,\beta}^{(\lambda)}\left(\frac{n+\alpha_2}{n+\beta_2}\right)=\left(\frac{n+\beta_2}{n}\right)\left\{\left[n-\alpha\beta+\lambda\frac{n}{n+\beta_2}\right]\left(\psi_{n-\alpha\beta,\beta}-\psi_{n-\alpha\beta-1,\beta}\right)\right.$$

$$\left.+\left[\beta+\lambda\frac{n}{n+\beta_2}\right]\left(\psi_{n-\alpha\beta,\beta}-\psi_{n-\alpha\beta,\beta-1}\right)\right\}.$$

Proof. The terms corresponding to $j=0$ and $j=\beta$ are first calculated separately.

$$\frac{d}{dx}P_{\beta,0}(x)=-\beta\left(\frac{n+\alpha_2}{n+\beta_2}-x\right)^{\beta-1}\text{ and }\frac{d}{dx}P_{\beta,\beta}(x)=\beta\left(x-\frac{\alpha_2}{n+\beta_2}\right)^{\beta-1}.$$

For the intermediate indices $1\le j\le\ \beta-1$, the following derivative relation is used:

$$\frac{d}{dx}P_{\beta,j}(x)=\beta\left[P_{\beta-1,j-1}(x)-P_{\beta-1,j}(x)\right].$$

The derivatives for the endpoint indices are as follows:

$$\frac{d}{dx}P_{\beta,0}^{(\lambda)}\left(\frac{\alpha_2}{n+\beta_2}\right)=-\left(\frac{n}{n+\beta_2}\right)^{\beta-1}\left[\beta+\lambda\left(\frac{n}{n+\beta_2}\right)\right],$$

$$\frac{d}{dx}P_{\beta,\beta}^{(\lambda)}\left(\frac{n+\alpha_2}{n+\beta_2}\right)=\left(\frac{n}{n+\beta_2}\right)^{\beta-1}\left[\beta+\lambda\left(\frac{n}{n+\beta_2}\right)\right].$$

For intermediate indices $1\le j\le\beta-1$,

$$\frac{d}{dx}P_{\beta,j}^{(\lambda)}(x)=P_{\beta,j}'(x)+\lambda\left(\frac{\beta-2j+1}{\beta^2-1}P_{\beta+1,j}'(x)-\frac{\beta-2j-1}{\beta^2-1}P_{\beta+1,j+1}'(x)\right).$$

Substituting these relations into the derivative formula for the intermediate indices yields the following endpoint values.

For $x=\frac{\alpha_2}{n+\beta_2}$ at the left end point, if $j\ge 2,\ j=1$, $\frac{d}{dx}P_{\beta,j}^{(\lambda)}\left(\frac{\alpha_2}{n+\beta_2}\right)=0$ and $\frac{d}{dx}P_{\beta,1}^{(\lambda)}\left(\frac{\alpha_2}{n+\beta_2}\right)=\left(\frac{n}{n+\beta_2}\right)^{\beta-1}\left[\beta+\lambda\frac{n}{n+\beta_2}\right]$.

At the left endpoint $x_0=\frac{\alpha_2}{n+\beta_2}$, the following values are obtained. For $j\ge 2$,

$$\frac{d}{dx}P_{\beta,j}^{(\lambda)}\left(\frac{\alpha_2}{n+\beta_2}\right)=0\,,$$

whereas for $j=1$,

$$\frac{d}{dx}P_{\beta,1}^{(\lambda)}\left(\frac{\alpha_2}{n+\beta_2}\right)=\left(\frac{n}{n+\beta_2}\right)^{\beta-1}\left[\beta+\lambda\frac{n}{n+\beta_2}\right].$$

At the right endpoint $x_1=\frac{n+\alpha_2}{n+\beta_2}$, for $j=\beta-1$, the following value is obtained:

$$\frac{d}{dx}P_{\beta,\beta-1}^{(\lambda)}\left(\frac{n+\alpha_2}{n+\beta_2}\right)=\left(\frac{n}{n+\beta_2}\right)^{\beta-1}\left[-\beta+\lambda\frac{n}{n+\beta_2}\right].$$

Similar equations are obtained for the other basis function as well.

$$P_{n-\alpha\beta,k}^{(\lambda)}{}'\left(\frac{\alpha_2}{n+\beta_2}\right)=0,\qquad k\geq 2,\qquad P_{\beta,j}^{(\lambda)}{}'\left(\frac{\alpha_2}{n+\beta_2}\right)=0,\qquad j\geq 2.$$

Therefore, the derivative at the left endpoint is obtained as

$$\frac{d}{dx}\mathfrak{B}_{n,\alpha,\beta}^{(\lambda)}\left(\frac{\alpha_2}{n+\beta_2}\right)=\left(\frac{n+\beta_2}{n}\right)\left\{\left[n-\alpha\beta+\lambda\frac{n}{n+\beta_2}\right]\left(\psi_{1,0}-\psi_{0,0}\right)\right.$$
$$\left.+\left[\beta+\lambda\frac{n}{n+\beta_2}\right]\left(\psi_{0,1}-\psi_{0,0}\right)\right\}.$$

At the right endpoint $x_1=\frac{n+\alpha_2}{n+\beta_2}$, the endpoint values of the basis functions imply that $P_{\beta,j}^{(\lambda)}\left(\frac{n+\alpha_2}{n+\beta_2}\right)=0, k\neq n-\alpha\beta$ and $P_{n-\alpha\beta,k}^{(\lambda)}\left(\frac{n+\alpha_2}{n+\beta_2}\right)=0, j\neq\beta$. Thus, only the term with $k=n-\alpha\beta$ and $j=\beta$ remains in the double sum.

Moreover, the derivatives satisfy

$$P_{n-\alpha\beta,k}^{(\lambda)}{}'\left(\frac{n+\alpha_2}{n+\beta_2}\right)=0,\ \text{for } k\leq n-\alpha\beta-2,$$

$$P_{\beta,j}^{(\lambda)}{}'\left(\frac{n+\alpha_2}{n+\beta_2}\right)=0,\ \text{for } j\leq\beta-2.$$

By applying the same technique, the derivative at the right endpoint is obtained as

$$\frac{d}{dx}\mathfrak{B}_{n,\alpha,\beta}^{(\lambda)}\left(\frac{n+\alpha_2}{n+\beta_2}\right)=\left(\frac{n+\beta_2}{n}\right)\left\{\left[n-\alpha\beta+\lambda\frac{n}{n+\beta_2}\right]\left(\psi_{n-\alpha\beta,\beta}-\psi_{n-\alpha\beta-1,\beta}\right)\right.$$
$$\left.+\left[\beta+\lambda\frac{n}{n+\beta_2}\right]\left(\psi_{n-\alpha\beta,\beta}-\psi_{n-\alpha\beta,\beta-1}\right)\right\}.$$

Combining the left and right endpoint computations completes the proof.

One of the important geometric properties of Bézier-type curves is their invariance under affine

transformations. The relevant theorem is given below.
Property 3.1. (Affine invariance) The positivity of the basis functions, together with the partition of unity property, ensures that the Bézier-type curve is invariant under affine transformations.

This property implies that the curve is independent of the chosen affine coordinate system, in a manner similar to the method used in [25].

An important geometric property is that the curve remains contained within the convex hull defined by its control points. The result related to this property is given as follows.
Property 3.2. (Convex hull property) The image of the Bézier-type curve is contained in the convex hull of its control points. Equivalently, by setting $I = \left[\frac{\alpha_2}{n+\beta_2}, \frac{n+\alpha_2}{n+\beta_2}\right]$, one has

$$\mathfrak{B}_{n,\alpha,\beta}^{(\lambda)}(I) \subseteq ConvexHull\{\psi_{k,j}\}, j = 0,1,\dots,\beta \text{ and } k = 0,1,\dots,n-\alpha\beta,$$

$$\mathfrak{B}_{n,\alpha,\beta}^{(\lambda)}(I) = \left\{\mathfrak{B}_{n,\alpha,\beta}^{(\lambda)}(x) : x \in \left[\frac{\alpha_2}{n+\beta_2}, \frac{n+\alpha_2}{n+\beta_2}\right]\right\}.$$

The Bézier-type curve satisfies a symmetry property when the order of its control points is reversed.
Theorem 3.7. For control points $\psi_{k,j}$, if $\psi_{k,j} = \psi_{n-\alpha\beta-k,\beta-j}$ is satisfied, then the λ −modified double-sum Bézier-type curve $\mathfrak{B}_{n,\alpha,\beta}^{(\lambda)}(x)$ is symmetric; that is,

$$\mathfrak{B}_{n,\alpha,\beta}^{(\lambda)}(x) = \mathfrak{B}_{n,\alpha,\beta}^{(\lambda)}\left(\frac{n+2\alpha_2}{n+\beta_2} - x\right).$$

Remark 3.5. When $\lambda = 0$, the curve $\mathfrak{B}_{n,\alpha,\beta}^{(\lambda)}(x)$ reduces to the classical Bézier-type curve.

In the next section, visual representations are generated using the basis functions associated with the proposed operator within a Bézier-type framework. Python is used to construct the visual examples of the λ-modified double-sum Bézier-type curves.

4. Applications of the proposed method

In this section, the applicability of the proposed theoretical framework is illustrated through selected visual examples constructed within a Bézier-type representation. The visual models are generated by using the basis functions associated with the proposed λ-modified double-sum operator together with prescribed control points. In particular, vessel-like geometric representations and organic-form-like visual examples are presented to show the geometric flexibility of the proposed construction.

Vascular narrowing is associated with several biological, metabolic, environmental, and genetic factors, including endothelial dysfunction, lipid accumulation, smoking-related effects, dyslipidemia, and genetic predisposition [36–43]. In the present study, these biomedical mechanisms are not modeled directly; rather, they are mentioned only to motivate the consideration of vessel-width variation as a geometric phenomenon. Accordingly, the proposed λ-modified double-sum Bézier-type construction is used to generate illustrative vessel-like geometric representations based on selected control points.

Bernstein basis functions are among the fundamental mathematical tools in computer-aided geometric design (CAGD), particularly because of their role in polynomial approximation and geometric modeling [44]. They are widely used in the construction of Bézier curves and surfaces, where control points provide a flexible and stable mechanism for shaping geometric forms [45].

Bernstein-based Bézier representations support the construction of complex geometric shapes through useful properties, such as the convex hull property and endpoint interpolation [46].

These features are useful in modeling natural and organic forms, such as plants and trees, which exhibit complex repetitive geometries requiring continuity and smoothness [47,48]. Furthermore, shape parameters allow curve shapes to be adjusted without changing the control polygon, thereby providing additional flexibility in geometric modeling [49]. Bernstein and Bézier representations also play an important role in basis conversion algorithms. For instance, B-spline curves can be decomposed into Bézier segments, and this decomposition is widely used in geometric modeling systems [50].

In the field of image processing, Bernstein polynomial-based methods have been used for image enhancement and reconstruction tasks due to their interpolation and approximation properties. In this context, methods based on the derivatives of Bernstein polynomials can provide more controlled gray-level transformations in image enhancement processes [51]. Recent studies also indicate that Bernstein operators may be used not only for image enhancement but also in areas such as image transfer and data security [19]. In particular, generalized Bézier-type representations in image space can support continuous and geometrically meaningful transformations between images [52]. Such approaches provide a mathematical basis for certain image transformation techniques and may help preserve selected structural and geometric properties during the transformation process [53].

Overall, Bernstein-based functions, operators, and Bézier representations remain active research topics because of their flexibility in natural shape generation, parametric modeling, image enhancement, and visual transfer [44,54]. In the present study, the visual examples illustrate how the proposed λ-modified double-sum Bézier-type construction can generate controlled geometric representations based on selected control points. In particular, vessel-like narrowing and widening patterns are considered only as geometric visualization examples, not as clinical, diagnostic, or patient-specific models [55]. These visualizations are not intended to replace validated clinical imaging techniques, such as MRI, CT, or angiography, or clinical assessment by a specialist physician [56].

Figure 9 presents a visualization of a vessel-like geometric model generated using λ-modified double-sum Bézier-type curves. It illustrates how different values of λ, such as (-0.5), (0.0), and (0.5), influence the generated shape, particularly in regions representing narrowing. The control points define the centerline, and normal vectors generate the boundaries of the vessel-like structure. This example demonstrates geometric narrowing and widening behavior in a controlled mathematical setting.

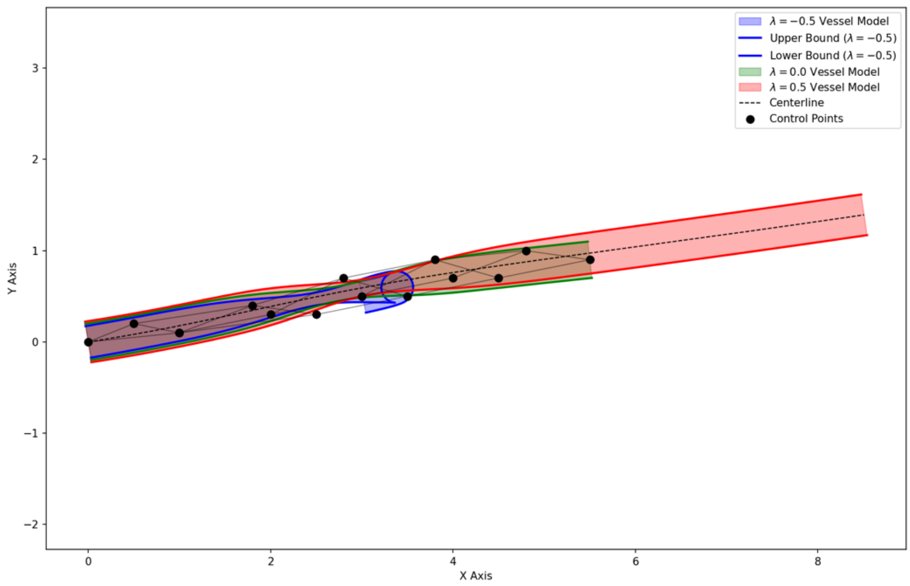

Figure 9. λ-modified vessel-like geometric model with narrowing and widening effects.

Figure 10 presents vessel-like geometric models generated using λ-modified double-sum Bézier-type curves. It illustrates how the lumen-like region and boundary curves vary for different values of λ, such as (-0.5), (0.0), and (0.5). These examples demonstrate the geometric flexibility of the proposed construction in representing narrowing- and widening-like patterns.

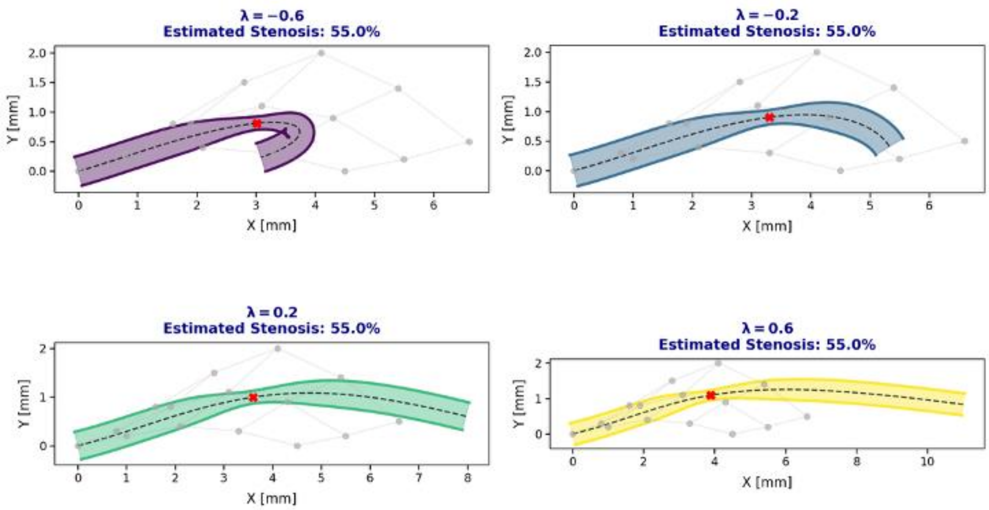

Figure 10. λ-modified vessel-like geometric models: Narrowing and widening patterns.

Figure 11 illustrates how the radius of the vessel-like geometry changes along its length for different values of the λ parameter. Different λ values affect the generated narrowing- and widening-like regions, thereby demonstrating how the proposed construction can control geometric variations in a mathematical visualization setting.

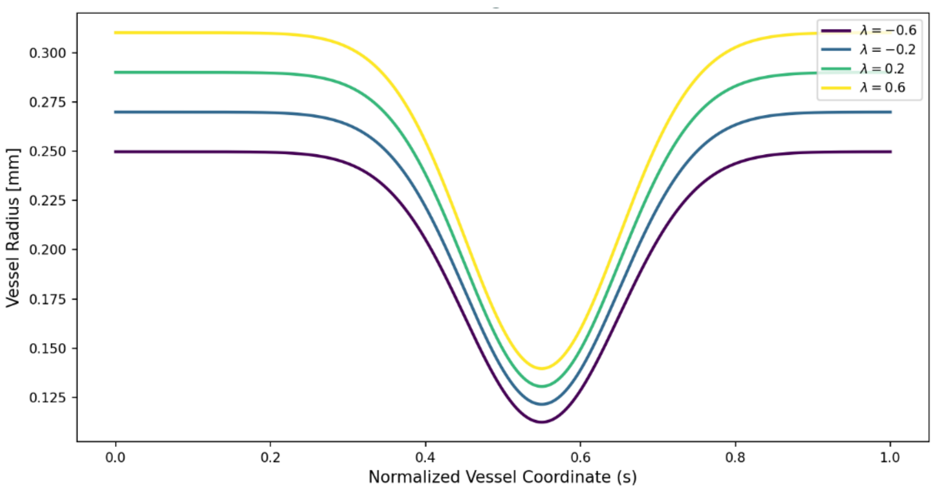

Figure 11. Radius distribution along the vessel-like geometry for different values of λ.

The following part presents visual elements generated using control points to illustrate the geometric flexibility of the proposed operator.

Figure 12 presents butterfly wing-like visual forms generated using the double-sum λ-modified Bézier-type curve model. The example illustrates how different λ parameters can affect the upper and lower wing geometries. In this context, the proposed construction serves as a geometric representation tool for generating complex visual forms based on prescribed control points. The example is intended to demonstrate visual flexibility rather than to make a quantitative claim regarding image transmission accuracy or simulation performance.

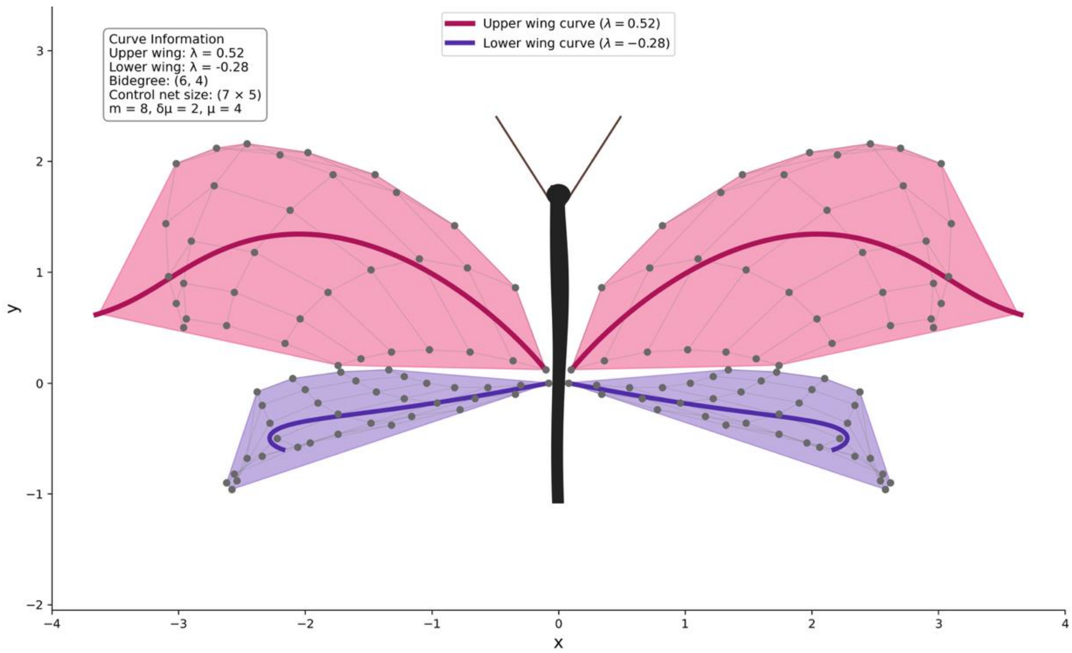

Figure 12. Butterfly wings generated by double-sum λ-modified Bézier-type curves.

The four matrices containing the control points for the butterfly wings illustrated in Figure 12 are presented in Table 1–4.

Table 1. Control point matrix $P_{\text{upper, right}}$.

.	$j = 0$	$j = 1$	$j = 2$	$j = 3$	$j = 4$
$k = 0$	(0.10, 0.12)	(0.34, 0.86)	(0.82, 1.42)	(1.45, 1.88)	(2.20, 2.06)
$k = 1$	(0.36, 0.20)	(0.72, 1.04)	(1.28, 1.72)	(1.98, 2.08)	(2.70, 2.12)
$k = 2$	(0.70, 0.28)	(1.10, 1.12)	(1.78, 1.88)	(2.46, 2.16)	(3.02, 1.98)
$k = 3$	(1.02, 0.30)	(1.48, 1.02)	(2.12, 1.56)	(2.72, 1.78)	(3.10, 1.44)
$k = 4$	(1.32, 0.28)	(1.82, 0.82)	(2.40, 1.18)	(2.90, 1.28)	(3.08, 0.96)
$k = 5$	(1.56, 0.22)	(2.04, 0.58)	(2.56, 0.82)	(2.96, 0.90)	(3.02, 0.72)
$k = 6$	(1.74, 0.16)	(2.16, 0.36)	(2.62, 0.52)	(2.94, 0.58)	(2.96, 0.50)

Table 2. Control point matrix $P_{\text{upper,left}}$.

	$j = 0$	$j = 1$	$j = 2$	$j = 3$	$j = 4$
$k = 0$	(-0.10, 0.12)	(-0.34, 0.86)	(-0.82, 1.42)	(-1.45, 1.88)	(-2.20, 2.06)
$k = 1$	(-0.36, 0.20)	(-0.72, 1.04)	(-1.28, 1.72)	(-1.98, 2.08)	(-2.70, 2.12)
$k = 2$	(-0.70, 0.28)	(-1.10, 1.12)	(-1.78, 1.88)	(-2.46, 2.16)	(-3.02, 1.98)
$k = 3$	(-1.02, 0.30)	(-1.48, 1.02)	(-2.12, 1.56)	(-2.72, 1.78)	(-3.10, 1.44)
$k = 4$	(-1.32, 0.28)	(-1.82, 0.82)	(-2.40, 1.18)	(-2.90, 1.28)	(-3.08, 0.96)
$k = 5$	(-1.56, 0.22)	(-2.04, 0.58)	(-2.56, 0.82)	(-2.96, 0.90)	(-3.02, 0.72)
$k = 6$	(-1.74, 0.16)	(-2.16, 0.36)	(-2.62, 0.52)	(-2.94, 0.58)	(-2.96, 0.50)

Table 3. Control point matrix $P_{\text{lower, right}}$.

	$j = 0$	$j = 1$	$j = 2$	$j = 3$	$j = 4$
$k = 0$	(0.08, 0.00)	(0.34, -0.10)	(0.78, -0.24)	(1.32, -0.38)	(1.96, -0.54)
$k = 1$	(0.30, -0.02)	(0.66, -0.14)	(1.16, -0.30)	(1.74, -0.46)	(2.34, -0.66)
$k = 2$	(0.56, -0.04)	(0.96, -0.18)	(1.48, -0.36)	(2.06, -0.58)	(2.56, -0.82)
$k = 3$	(0.82, -0.04)	(1.22, -0.14)	(1.74, -0.28)	(2.22, -0.50)	(2.62, -0.90)
$k = 4$	(1.04, 0.00)	(1.44, -0.08)	(1.90, -0.18)	(2.28, -0.36)	(2.58, -0.96)
$k = 5$	(1.22, 0.06)	(1.60, 0.02)	(2.00, -0.06)	(2.34, -0.20)	(2.54, -0.88)
$k = 6$	(1.34, 0.12)	(1.72, 0.10)	(2.10, 0.04)	(2.38, -0.08)	(2.46, -0.68)

Table 4. Control point matrix $P_{\text{lower, left}}$.

	$j = 0$	$j = 1$	$j = 2$	$j = 3$	$j = 4$
$k = 0$	(-0.08, 0.00)	(-0.34, -0.10)	(-0.78, -0.24)	(-1.32, -0.38)	(-1.96, -0.54)
$k = 1$	(-0.30, -0.02)	(-0.66, -0.14)	(-1.16, -0.30)	(-1.74, -0.46)	(-2.34, -0.66)
$k = 2$	(-0.56, -0.04)	(-0.96, -0.18)	(-1.48, -0.36)	(-2.06, -0.58)	(-2.56, -0.82)
$k = 3$	(-0.82, -0.04)	(-1.22, -0.14)	(-1.74, -0.28)	(-2.22, -0.50)	(-2.62, -0.90)
$k = 4$	(-1.04, 0.00)	(-1.44, -0.08)	(-1.90, -0.18)	(-2.28, -0.36)	(-2.58, -0.96)
$k = 5$	(-1.22, 0.06)	(-1.60, 0.02)	(-2.00, -0.06)	(-2.34, -0.20)	(-2.54, -0.88)
$k = 6$	(-1.34, 0.12)	(-1.72, 0.10)	(-2.10, 0.04)	(-2.38, -0.08)	(-2.46, -0.68)

The algorithmic steps presented in Table 5 summarize the construction of the butterfly model using the proposed double-sum λ-modified Bézier-type curve approach.

Table 5. Algorithm steps.

Step	Description
1	Definition of Model Parameters
2	Determination of Effective Degrees
3	Definition of the Parameter Interval
4	Specification of the Upper and Lower Wing λ-Parameters
5	Construction of the Right-Wing Control Nets
6	Generation of the Left-Wing Control Nets by Symmetry
7	Definition of the Classical Bernstein-Type Basis Function
8	Definition of the λ-Modified Basis Function
9	Construction of the Double-Sum λ-Modified Bézier-Type Curve
10	Sampling of the Parameter Interval
11	Evaluation of the Upper Wing Curves
12	Evaluation of the Lower Wing Curves
13	Construction of the Filled Wing Regions
14	Computation of the Convex Hulls of the Control Points
15	Construction of the Butterfly Body
16	Construction of the Head and Antennae
17	Drawing of the Control Nets
18	Annotation of the Upper and Lower Wing Curves
19	Visualization of the Butterfly Model
20	Export of the Final Butterfly Figure

Figure 13 presents a leaf-like geometric form generated using double-sum λ-modified Bézier-type curves. The model illustrates how selected control points and the λ parameter represent the outer boundary, internal curvature, and vein-like structures of an organic form. This example demonstrates the geometric flexibility of the proposed construction in generating organic visual representations, rather than providing a biologically exact leaf model.

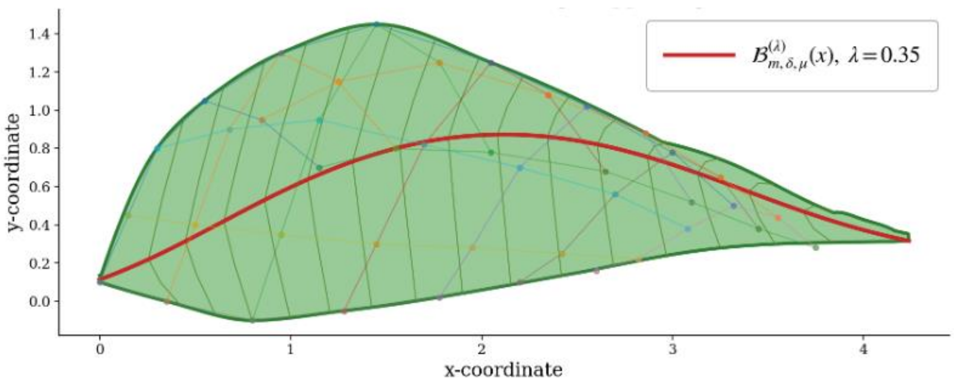

Figure 13. Leaf model generated by double-sum λ-modified Bézier-type curves.

The matrix of control points for the leaf drawing shown in Figure 13 is presented in Table 6:

Table 6. Control point matrix P_{leaf}.

	$j = 0$	$j = 1$	$j = 2$	$j = 3$	$j = 4$	$j = 5$
$k = 0$	(0.00, 0.10)	(0.15, 0.45)	(0.30, 0.80)	(0.55, 1.05)	(0.85, 0.95)	(1.15, 0.70)
$k = 1$	(0.35, 0.00)	(0.50, 0.40)	(0.68, 0.90)	(0.95, 1.30)	(1.25, 1.15)	(1.55, 0.80)
$k = 2$	(0.80, -0.10)	(0.95, 0.35)	(1.15, 0.95)	(1.45, 1.45)	(1.78, 1.25)	(2.05, 0.78)
$k = 3$	(1.28, -0.05)	(1.45, 0.30)	(1.70, 0.82)	(2.05, 1.25)	(2.35, 1.08)	(2.65, 0.68)
$k = 4$	(1.78, 0.02)	(1.95, 0.28)	(2.20, 0.70)	(2.55, 1.02)	(2.86, 0.88)	(3.10, 0.52)
$k = 5$	(2.20, 0.10)	(2.42, 0.25)	(2.70, 0.56)	(3.00, 0.78)	(3.25, 0.65)	(3.45, 0.38)
$k = 6$	(2.60, 0.16)	(2.82, 0.22)	(3.08, 0.38)	(3.32, 0.50)	(3.55, 0.44)	(3.75, 0.28)

4.1. Organic form and vessel-like geometric representation using λ-modified double-sum Bézier-type curves

The proposed λ-modified double-sum Bézier-type construction can generate organic-form-like visual representations, such as leaf-like and butterfly-wing-like geometries, through selected control points. In this setting, the λ parameter provides an additional degree of geometric flexibility, allowing changes in features such as boundary curvature, local widening, and vein-like internal structures. These examples illustrate the visual and geometric flexibility of the proposed construction, rather than providing biologically exact models of natural objects.

From a geometric visualization perspective, λ-parameterized Bézier-type curves can also represent vessel-like shapes with narrowing- and widening-like regions [57,58].

4.2. Curvature-based geometric representation and educational visualization

In the proposed vessel-like geometric examples, the λ parameter adjusts curvature and local radius variation in the generated shapes. Thus, the model can visualize narrowing-and widening-like geometric patterns in a controlled mathematical setting.

In the present study, however, the generated vessel-like forms serve only as illustrative geometric examples. More realistic vascular modeling would require patient-specific anatomical data, tissue properties, blood viscosity, hemodynamic analysis, and clinical validation, which are beyond the scope of the present work.

4.3. Scope and limitations of the illustrative examples

It should be emphasized that all vessel-like and organic-form-like examples presented in this section are mathematical and geometric visualizations generated by the proposed λ-modified double-sum Bézier-type construction. They are not based on patient-specific imaging data, blood-flow measurements, tissue properties, physiological parameters, or biological validation. Therefore, they should not be considered for clinical decision-making, diagnostic models, surgical planning, medical imaging training tools, clinical education platforms, blood-flow analyses, or validated biomedical simulations. More realistic biomedical modeling would require patient-specific anatomical data, hemodynamic analysis, tissue properties, and clinical validation, which are beyond the scope of the present study.

5. Results and discussion

In this study, a λ-modified DD Stancu-type double-sum operator was constructed and examined from both approximation-theoretic and geometric perspectives. The basis functions associated with the operator were analyzed in terms of positivity, partition of unity, linear independence, unimodality, endpoint behavior, and Bézier-type geometric representation. In addition, Korovkin-type convergence and related approximation properties were obtained, and selected visual examples were generated to illustrate the effect of the parameter λ on the resulting geometric forms.

The results indicate that the parameter λ provides an additional degree of flexibility in the proposed construction. In the approximation-theoretic setting, different values of λ affect the behavior of the corresponding operator and its approximation performance. In the geometric setting, the same parameter contributes to controlled variations in vessel-like, leaf-like, and butterfly-wing-like visual forms generated from prescribed control points.

The vessel-like visual examples are intended only as geometric representations generated by the proposed Bézier-type construction. They do not involve patient-specific vascular data, clinical imaging, hemodynamic simulation, or diagnostic validation. Therefore, they are presented as illustrative geometric examples rather than clinical or biomedical decision-support tools.

The organic-form-like examples indicate that the basis functions associated with the proposed operator can be used in Bézier-type constructions to generate flexible visual representations. These examples are intended to show geometric flexibility rather than biological accuracy or quantitative modeling performance.

5.1. Research and preliminary geometric exploration

The generated visual examples may support preliminary exploration of geometric relationships between shape parameters and the resulting forms. In the vessel-like examples, variations in the parameter λ allow narrowing-like, widening-like, and curvature-related patterns to be visualized in a controlled mathematical setting. In the organic-form-like examples, similar parameter variations affect boundary curvature and internal vein-like structures.

In this context, the examples may support the formulation of geometric hypotheses concerning the relationship between control points, shape parameters, and generated forms. Related geometry-editing approaches in the literature suggest that geometric modifications can be useful for exploring form-function relationships in biological systems [59–65]. However, the present study does not involve patient-specific morphology analysis, blood-flow simulation, or clinical validation; the examples are limited to illustrative Bézier-type geometric representations.

Computational geometry-editing approaches may support the development of geometric hypotheses by visualizing the effects of structural modifications on generated forms [60,65].

Parameter effects in geometric representations: By examining how parameters such as λ affect the shape of curves and surfaces, the proposed construction provides an intuitive geometric understanding of parameter-dependent form variation.

Shape parameters provide flexible control over curves and surfaces, while geometric modifications allow the construction of visual forms inspired by real-world shapes [56,66].

Visualization tools can be useful for communicating complex concepts in areas such as geometric modeling, computer-aided design, biomechanics, and mathematical analysis through visual representations [65,66].

Educational visualization context: Visualization-based approaches may support the conceptual understanding of geometric and anatomical forms in educational settings [66,67]. In the present study, however, the generated vessel-like and organic-form-like examples work only as illustrative geometric representations. They are not intended as medical imaging training tools, clinical simulation systems, or educational platforms for diagnosing vascular abnormalities.

Although the parameter λ is used in the present study as a mathematical shape-control parameter, its possible connection with biophysical factors may be considered in future extensions. In real vascular environments, the apparent narrowing or widening of a vessel is not determined by geometry alone, but may also be affected by blood viscosity, local flow pressure, wall shear stress, vessel wall elasticity, and tissue deformation. These factors could influence how a geometric model adjusts its curvature, smoothness, or local constriction profile. Therefore, in a future biomechanically informed framework, λ may be investigated as an adjustable geometric proxy associated with such dynamic effects. However, establishing this connection would require real anatomical data, hemodynamic modeling, and clinical validation. Thus, the present work should be interpreted only as a preliminary mathematical and geometric representation.

5.2. Visualization and presentation

Scientific publications: The generated visual representations can present theoretical constructions and geometric examples clearly and understandably in scientific articles and presentations.

Design and art: Owing to the shape-control properties of curves and surfaces, the proposed Bézier-type construction may also generate visually varied geometric forms.

Curves and surfaces with shape-control properties are widely used in visual design and in the construction of varied geometric forms [46,68].

Contribution to geometric modeling: The examples indicate that the proposed λ-modified double-sum Bézier-type construction can generate flexible geometric representations in computer graphics and geometric modeling. In particular, leaf-like and other organic-form-like structures can be represented through prescribed control points and parameter-dependent shape variation.

In conclusion, the hybrid operator introduced in this study combines the DD Stancu-type structure with the λ-parameter modification. The results show that the proposed construction preserves the geometric interpretability of the basis-function framework while providing additional flexibility through λ. Together, the theoretical results and visual examples indicate that the operator may be useful for approximation-theoretic analysis and Bézier-type geometric representation.

Finally, possible extensions of the proposed operator, including neutrosophic generalizations, may be considered in future studies, particularly in connection with decision-making frameworks such as the method discussed in [69]. Recent developments in approximation theory indicate that parameter-dependent positive linear operators continue to provide flexible tools for convergence analysis, error estimation, and shape-preserving approximation. In this direction, future studies may compare the proposed hybrid DD Stancu operator with recent Bernstein-Kantorovich-Stancu, q-Schurer-type, beta-type Szász-Mirakjan, and GBS-associated operator families [70–73]. Such comparisons may further clarify the approximation performance, geometric flexibility, and potential application-oriented advantages of the proposed construction.

Beyond its theoretical contribution to approximation theory and geometric modeling, the hybrid-type Stancu operator may also offer a promising mathematical basis for future applications in multimedia security and secure image transmission. Recent studies on multimedia security show that rigorous image and video protection requires not only visual transformation but also cryptographic design and security evaluation. For example, chaos-based S-box structures, cryptanalysis-driven improvements, and hyperchaotic image encryption schemes have been developed to enhance confusion, diffusion, key sensitivity, and resistance against attacks. In this context, the proposed hybrid operator should not be regarded as a standalone encryption method. Instead, it may be considered a mathematical and geometric representation tool that could potentially support preprocessing or structural transformation stages in future secure image transmission frameworks. A complete security-oriented extension of the present approach would require standard analyses such as information entropy, adjacent-pixel correlation, key-space analysis, NPCR/UACI, robustness against differential attacks, and computational complexity evaluation. The cryptanalysis and improvement of chaos- and S-box-based video cryptosystems reported in [74], along with the design and application of 3D non-degenerate hyperchaotic systems for image encryption presented in [75], offer security-oriented perspectives on this subject. In future studies on image encryption using the proposed operator, the comprehensive cryptographic and statistical security analyses provided in these two papers could offer valuable perspectives.

6. Conclusions

In this study, a novel λ-modified DD Stancu-type double-sum operator was constructed and analyzed, establishing a connection between approximation theory and geometric modeling. The basis functions associated with the proposed operator were shown to satisfy fundamental properties, including positivity, partition of unity, and linear independence. These properties are essential for both theoretical convergence analysis and the practical construction of Bézier-type curves. The parameter λ was identified as an effective mathematical shape-control parameter that provides additional geometric flexibility. This flexibility enables the operator to represent organic-like forms, such as vessel geometries, leaf contours, and butterfly-wing patterns, with a high degree of visual accuracy. The theoretical results demonstrated that the operator satisfies a Korovkin-type convergence theorem, thereby ensuring reliable approximation behavior. In addition, the geometric examples illustrated the direct influence of λ on curvature, smoothness, and local constriction profiles. It should be emphasized that the vascular visualizations presented in this study are purely geometric representations and should not be interpreted as clinical simulations, diagnostic tools, or validated hemodynamic models. Similarly, the botanical and entomological examples are intended to demonstrate the geometric flexibility of the proposed method rather than to provide biologically accurate reconstructions.

Future research may investigate the potential biophysical interpretation of λ by incorporating real anatomical data, hemodynamic parameters, and tissue-mechanical properties. However, such extensions would require rigorous experimental and clinical validation. Overall, this study introduces a flexible mathematical framework for geometric design and provides a promising basis for future interdisciplinary research integrating approximation theory with biomechanical modeling.

Author contributions

Nazmiye Gonul Bilgin: Conceptualization, Methodology, Supervision, Validation, Writing—review and editing. Emine Guven: Writing—original draft, Data curation, Validation, Visualization, Writing—review and editing. All authors have read and agreed to the published version of the manuscript.

Use of Generative-AI tools declaration

The authors declare they have used Artificial Intelligence (AI) tools in the creation of this article.

Acknowledgments

This work is a further development of one of the operators introduced in the first author's PhD thesis (in Chapter 7), completed at Zonguldak Bülent Ecevit University in June 2026 under the supervision of the second author, and extends that operator by incorporating an application-oriented

aspect.

Conflict of interest

The authors declare no conflict of interest.

References

1. K. Weierstrass, Über die analytische Darstellbarkeit sogenannter willkürlicher Functionen einer reellen Veränderlichen, In: *Sitzungsberichte der Königlich Preußischen Akademie der Wissenschaften zu Berlin*, 1885, 789–805.
2. S. Bernstein, Démonstration du théorème de Weierstrass fondée sur le calcul des probabilités, *Soobshch. Khar'k. Mat. Obs.*, **13** (1912), 1–2.
3. G. G. Lorentz, *Bernstein polynomials*, 1953.
4. P. Bézier, *Numerical control: mathematics and applications*, Translated by AR Forrest, 1972).
5. P. de Casteljau, *Outillages méthodes calcul*, Technical Report, Paris: André Citroën Automobiles SA, 1959.
6. T. Lyche, J. L. Merrien, Bézier curves and Bernstein polynomials, In: *Exercises in Computational Mathematics with MATLAB*, Berlin: Springer, 2014. https://doi.org/10.1007/978-3-662-43511-3_7
7. J. Hoschek, D. Lasser, *Fundamentals of computer aided geometric design*, 1993.
8. L. V. Kantorovich, Sur certains développements suivant les polynômes de la forme de S. *Bernstein, I, II, C. R. Acad. URSS*, **563** (1930), 595–600.
9. I. Chlodowsky, Sur le développement des fonctions définies dans un intervalle infini en séries de polynomes de M. S. Bernstein, *Compos. Math.*, **4** (1937), 380–393.
10. J. L. Durrmeyer, *Une formule d'inversion de la transformée de Laplace: Applications à la théorie des moments*, 1967.
11. D. D. Stancu, Approximation of functions by a new class of polynomial operators, *Rev. Roum. Math. Pures*, **13** (1968), 1173–1194.
12. G. M. Phillips, On generalized Bernstein polynomials, In: *Numerical Analysis: A. R. Mitchell 75th Birthday Volume*, 1996, 263–269. https://doi.org/10.1142/9789812812872_0018
13. V. Gupta, R. P. Agarwal, *Convergence estimates in approximation theory*, Swıtzerland: Springer, 2014. https://doi.org/10.1007/978-3-319-02765-4
14. V. A. Baskakov, An instance of a sequence of linear positive operators in the space of continuous functions, *Dokl. Akad. Nauk SSSR*, **113** (1957), 249–251.
15. F. Schurer, *Linear positive operators in approximation theory*, 1965.
16. A. D. Gadjiev, A. M. Ghorbanalizadeh, Approximation properties of a new type Bernstein-Stancu polynomials of one and two variables, *Appl. Math. Comput.*, **216** (2010), 890–901. https://doi.org/10.1016/j.amc.2010.01.099
17. S. Yıldız, N. S. Bayram, On P-equi-statistical relative convergence in sequences of fuzzy-valued functions with applications to Korovkin-type approximation, *Filomat*, **39** (2025), 11621–11636. https://doi.org/10.2298/FIL2532621Y

18. M. Mursaleen, K. J. Ansari, A. Khan, Some approximation results by (*p, q*)-analogue of Bernstein-Stancu operators, *Appl. Math. Comput.*, **264** (2015), 392–402. https://doi.org/10.1016/j.amc.2015.03.135
19. N. G. Bilgin, Y. Kaya, M. Eren, Security of image transfer and innovative results for (*p, q*)-Bernstein-Schurer operators, *AIMS Math.*, **9** (2024), 23812–23836. https://doi.org/10.3934/math.20241157
20. S. Herdem, S. Erkovan, On the construction of iterative methods in (*p,q*)-calculus, *Numer. Algor.*, 2026. https://doi.org/10.1007/s11075-025-02300-9
21. G. Icoz, A Kantorovich variant of a new type Bernstein-Stancu polynomials, *Appl. Math. Comput.*, **218** (2012), 8552–8560. https://doi.org/10.1016/j.amc.2012.02.017
22. N. G. Bilgin, E. Güven, On a new type of DD Stancu operators, In: *14th International Conference on Engineering and Natural Sciences*, 2022.
23. G. Bascanbaz-Tunca, A note on Stancu operators with three parameters, *Bull. Transilv. Univ. Brasov Ser. III*, **67** (2025), 55–70. https://doi.org/10.31926/but.mif.2025.5.67.1.4
24. A. Alotaibi, On the approximation process of shifted-knots bivariate Stancu-type Kantorovich operators, *J. Math.*, **2026** (2026), 8454636. https://doi.org/10.1155/jom/8454636
25. Z. Ye, X. Long, X. M. Zeng, Adjustment algorithms for Bézier curve and surface, In: *2010 5th International Conference on Computer Science and Education*, China, 2010, 1712–1716. https://doi.org/10.1109/ICCSE.2010.5593563
26. Q. B. Cai, B. Y. Lian, G. Zhou, Approximation properties of λ-Bernstein operators, *J. Inequal. Appl.*, **2018** (2018), 6. https://doi.org/10.1186/s13660-018-1653-7
27. Q. Cai, R. Aslan, Note on a new construction of Kantorovich form q-Bernstein operators related to shape parameter λ, *Comput. Model. Eng. Sci.,* **130** (2022), 1479–1493. https://doi.org/10.32604/cmes.2022.018338
28. M. Ayman-Mursaleen, M. Nasiruzzaman, N. Rao, M. Dilshad, K. S. Nisar, Approximation by the modified λ-Bernstein-polynomial in terms of basis function, *AIMS Math.*, **9** (2024), 4409–4426. https://doi.org/10.3934/math.2024217
29. X. L. Qiu, M. Bodur, Q. B. Cai, A Bézier variant of (λ,μ)-Bernstein-Kantorovich-Stancu operators, *J. Inequal. Appl.*, **2026** (2026), 21. https://doi.org/10.1186/s13660-026-03436-5
30. Q. B. Cai, G. Torun, Ü. Dinlemez Kantar, Approximation properties of generalized λ-Bernstein-Stancu-type operators, *J. Math.*, **2021** (2021), 5590439. https://doi.org/10.1155/2021/5590439
31. T. Acar, A. Aral, Weighted approximation by new Bernstein-Chlodowsky-Gadjiev operators, *Filomat*, **27** (2013), 371–380. https://doi.org/10.2298/FIL1302371A
32. M. Mursaleen, K. J. Ansari, A. Khan, Approximation by Kantorovich type *q*-Bernstein-Stancu operators, *Complex Anal. Oper. Theory*, **11** (2017), 85–107. https://doi.org/10.1007/s11785-016-0572-1
33. R. Yang, J. Xiong, F. Cao, Multivariate Stancu operators defined on a simplex, *Appl. Math. Comput.*, **138** (2003), 189–198. https://doi.org/10.1016/S0096-3003(02)00088-7
34. Z. P. Lin, G. Torun, E. Kangal, Ü. D. Kantar, Q. B. Cai, On the properties of the modified λ-Bernstein-Stancu operators, *Symmetry*, **16** (2024), 1276. https://doi.org/10.3390/sym16101276
35. V. Gupta, Kantorovich variant of Stancu operators, *Filomat*, **36** (2022), 5107–5117. https://doi.org/10.2298/FIL2215107G

36. D. Malinowski, O. Bochniak, K. Luterek-Puszyńska, M. Puszyński, A. Pawlik, Genetic risk factors related to coronary artery disease and role of transforming growth factor beta 1 polymorphisms, *Genes*, **14** (2023), 1425. https://doi.org/10.3390/genes14071425
37. R. McPherson, A. Tybjaerg-Hansen, Genetics of coronary artery disease, *Circ. Res.*, **118** (2016), 564–578. https://doi.org/10.1161/CIRCRESAHA.115.306566
38. S. Zhang, I. Day, S. Ye, Nicotine induced changes in gene expression by human coronary artery endothelial cells, *Atherosclerosis*, **154** (2001), 277–283. https://doi.org/10.1016/S0021-9150(00)00475-5
39. B. Messner, D. Bernhard, Smoking and cardiovascular disease: mechanisms of endothelial dysfunction and early atherogenesis, *Arterioscler. Thromb. Vasc. Biol.*, **34** (2014), 509–515. https://doi.org/10.1161/ATVBAHA.113.300156
40. J. S. Hill, M. R. Hayden, J. Frohlich, P. H. Pritchard, Genetic and environmental factors affecting the incidence of coronary artery disease in heterozygous familial hypercholesterolemia, *Arterioscler. Thromb.*, **11** (1991), 290–297. https://doi.org/10.1161/01.ATV.11.2.290
41. M. G. Levin, D. Klarin, T. L. Assimes, M. S. Freiberg, E. Ingelsson, J. Lynch, et al., Genetics of smoking and risk of atherosclerotic cardiovascular diseases: A mendelian randomization study, *JAMA Netw. Open*, **4** (2021), e2034461. https://doi.org/10.1001/jamanetworkopen.2020.34461
42. A. V. Khera, C. A. Emdin, I. Drake, P. Natarajan, A. G. Bick, N. R. Cook, et al., Genetic risk, adherence to a healthy lifestyle, and coronary disease, *N. Engl. J. Med.*, **375** (2016), 2349–2358. https://doi.org/10.1056/NEJMoa1605086
43. N. L. Benowitz, A. D. Burbank, Cardiovascular toxicity of nicotine: Implications for electronic cigarette use, *Trends Cardiovas. Med.*, **26** (2016), 515–523. https://doi.org/10.1016/j.tcm.2016.03.001
44. A. Yilmaz Ceylan, B. Simsek, The formulae and symmetry property of Bernstein type polynomials related to special numbers and functions, *Symmetry*, **16** (2024), 1159. https://doi.org/10.3390/sym16091159
45. D. Canlı, S. Senyurt, Bézier curves and surfaces with the generalized α-Bernstein operator, *Symmetry*, **17** (2025), 187. https://doi.org/10.3390/sym17020187
46. G. E. Farin, *Curves and surfaces for CAGD: A practical guide*, Morgan Kaufmann, 2002.
47. A. Tas, G. Mutlu Avinc, Architectural designs inspired by nature and mathematical models, *Archit. Eng.*, **10** (2025), 3–14. https://doi.org/10.23968/2500-0055-2025-10-3-3-14
48. P. Prusinkiewicz, A. Lindenmayer, *The algorithmic beauty of plants*, Springer-Verlag, 1990.
49. X. A. Han, Y. Ma, X. Huang, The cubic trigonometric Bézier curve with two shape parameters, *Appl. Math. Lett.*, **22** (2009), 226–231. https://doi.org/10.1016/j.aml.2008.03.015
50. L. Piegl, W. Tiller, *The NURBS book*, Springer Science & Business Media, 2012.
51. V. Pătrașcu, Gray level image enhancement using the Bernstein polynomials, 2014. https://doi.org/10.48550/arXiv.1412.5769
52. A. Effland, M. Rumpf, S. Simon, K. Stahn, B. Wirth, Bézier curves in the space of images, In: *Scale Space and Variational Methods in Computer Vision (SSVM 2015)*, Cham: Springer, 2015. https://doi.org/10.1007/978-3-319-18461-6_30
53. B. Berkels, A. Effland, M. Rumpf, Time discrete geodesic paths in the space of images, *SIAM J. Imaging Sci.*, **8** (2015), 1457–1488. https://doi.org/10.1137/140970719

54. S. Bashir, D. Ahmad, G. Ali, Exploring q-Bernstein-Bézier surfaces in Minkowski space: Analysis, modeling, and applications, *PLoS One*, **19** (2024), e0299892. https://doi.org/10.1371/journal.pone.0299892
55. D. F. Young, F. Y. Tsai, Flow characteristics in models of arterial stenoses—I. Steady flow, *J. Biomech.*, **6** (1973), 395–410. https://doi.org/10.1016/0021-9290(73)90099-7
56. E. J. Topol, High-performance medicine: the convergence of human and artificial intelligence, *Nat. Med.*, **25** (2019), 44–56. https://doi.org/10.1038/s41591-018-0300-7
57. I. Karakılıc, S. Karakılıc, G. Budakcı, F. Ozger, Bézier curves and surfaces with the blending (α,λ,s)-Bernstein basis, *Symmetry*, **17** (2025), 219. https://doi.org/10.3390/sym17020219
58. J. R. Cebral, F. Mut, D. Sforza, R. Löhner, E. Scrivano, P. Lylyk, et al., Clinical application of image-based CFD for cerebral aneurysms, *Int. J. Numer. Meth. Bio.*, **27** (2011), 977–992. https://doi.org/10.1002/cnm.1373
59. J. Egger, S. Grosskopf, C. Nimsky, T. Kapur, B. Freisleben, Modeling and visualization techniques for virtual stenting of aneurysms and stenoses, *Comput. Med. Imag. Grap.*, **36** (2012), 183–203. https://doi.org/10.1016/j.compmedimag.2011.12.002
60. J. Pham, S. Wyetzner, M. R. Pfaller, D. W. Parker, D. L. James, A. L. Marsden, svMorph: Interactive geometry-editing tools for virtual patient-specific vascular anatomies, *J. Biomech. Eng.*, **145** (2023), 031001. https://doi.org/10.1115/1.4056055
61. P. D. Morris, A. Narracott, H. von Tengg-Kobligk, D. A. S. Soto, S. Hsiao, A. Lungu, et al., Computational fluid dynamics modelling in cardiovascular medicine, *Heart*, **102** (2016), 18–28. https://doi.org/10.1136/heartjnl-2015-308044
62. J. R. Cebral, F. Mut, J. Weir, C. M. Putman, Association of hemodynamic characteristics and cerebral aneurysm rupture, *AJNR Am. J. Neuroradiol.*, **32** (2011), 264–270. https://doi.org/10.3174/ajnr.A2274
63. J. Eves, A. Sudarsanam, J. Shalhoub, D. Amiras, Augmented reality in vascular and endovascular surgery: Scoping review, *JMIR Serious Games*, **10** (2022), e34501. https://doi.org/10.2196/34501
64. E. Bullitt, G. Gerig, S. M. Pizer, W. Lin, S. R. Aylward, Measuring tortuosity of the intracerebral vasculature from MRA images, *IEEE T. Med. Imaging*, **22** (2003), 1163–1171. https://doi.org/10.1109/TMI.2003.816964
65. C. Ware, *Information visualization: Perception for design*, Elsevier, 2012.
66. V. G. Duffy, Human digital modeling in design, In: *Handbook of Human Factors and Ergonomics*, 2012, 1016–1030. https://doi.org/10.1002/9781118131350.ch35
67. A. Haiser, A. Aydin, B. Kunduzi, K. Ahmed, P. Dasgupta, A systematic review of simulation-based training in vascular surgery, *J. Surg. Res.,* **279** (2022), 409–419. https://doi.org/10.1016/j.jss.2022.05.009
68. R. I. Nabiyev, R. Ziatdinov, A mathematical design and evaluation of Bernstein-Bézier curves' shape features using the laws of technical aesthetics, *Math. Des. Tech. Aesthet.*, **2** (2014), 6–13.
69. N. G. Bilgin, G. Bozma, M. Riaz, Location selection criteria for a military base in border region using N-AHP method, *AIMS Math.*, **9** (2024), 7529–7551. https://doi.org/10.3934/math.2024365
70. A. Alotaibi, M. Nasiruzzaman, S. A. Mohiuddine, On the convergence of Bernstein-Kantorovich-Stancu shifted knots operators involving Schur parameter, *Complex Anal. Oper. Theory*, **18** (2024), 4. https://doi.org/10.1007/s11785-023-01423-y

71. M. Nasiruzzaman, A. Alotaibi, Kantorovich extension of parametric generalized q-Schurer operators and their approximation properties, *Mathematics*, **13** (2025), 3770. https://doi.org/10.3390/math13233770
72. Md. Nasiruzzaman, R. T. Alqahtani, S. A. Mohiuddine, Approximation properties of a new class of beta-type Szász-Mirakjan operators, *J. Math.*, **2025** (2025), 6680828. https://doi.org/10.1155/jom/6680828
73. Md. Nasiruzzaman, Approximation by GBS associated properties of Szász-Mirakjan-Jakimovski-Leviatan-Kantorovich operators, *Filomat*, **38** (2024), 6621–6637. https://doi.org/10.2298/FIL2418621N
74. Y. Lin, Y. Wei, D. Chen, Y. Li, U. Erkan, A. Toktaş, et al., Cryptanalysis and improvement of a video cryptosystem via chaos and S-box, *ACM T. Multim. Comput.*, **22** (2026), 1–28. https://doi.org/10.1145/3808699
75. Y. Lin, Y. Liao, W. Zeng, Y. Wei, D. Chen, X. Yuan, et al., 3D non-degenerate hyperchaos: Design, analysis, and application in image encryption, *IEEE T. Consum. Electr.*, 2026. https://doi.org/10.1109/TCE.2026.3672135

AIMS Press

© 2025 the Author(s), licensee AIMS Press. This is an open access article distributed under the terms of the Creative Commons Attribution License (https://creativecommons.org/licenses/by/4.0)